Carbon, iron and sulfur records of lacustrine paleo-environments during the middle Eocene in eastern China

Xinping Liang, Sergei Katsev, Quanyou Liu, Gleb S. Pokrovski, Zhijun Jin

Science of the Total Environment

Carbon, iron and sulfur records of lacustrine paleo-environments during the middle Eocene in eastern China

--Manuscript Draft--

Manuscript Number:	STOTEN-D-24-35639R2
Article Type:	Research Paper
Keywords:	organic carbon burial; ferruginous conditions; volcanism; transgression; paralic lacustrine shale; middle Eocene
Corresponding Author:	Xinping Liang Peking University CHINA
First Author:	Xinping Liang
Order of Authors:	Xinping Liang
	Sergei Katsev
	Quanyou Liu
	Gleb S. Pokrovski
	Zhijun Jin
Abstract:	It is widely recognized that anoxic conditions facilitate the preservation of organic carbon in marine sediments. However, the specific geological factors that lead to the development of such conditions in paleo-lakes are less well understood. Owing to their smaller size, paleolakes could experience more frequent and stronger changes in geochemical conditions than oceans. Such changes, such as volcanism, hydrothermal fluids, or ocean transgressions, can also strongly affect the lacustrine organic carbon burial thereby complicating sediment diagenesis record. Here, we used total organic carbon content (TOC), organic carbon isotope (δ13Corg), iron speciation, and pyrite sulfur isotope (δ34Spy) data to establish relationships between organic carbon preservation and anoxic conditions in fine-grained sediments from the middle Eocene lacustrine depositional environments from the Shahejie Formation of the Jiyang Depression, Bohai Bay Basin, eastern China. The results reveal TOC between 1% and 10%, highly-reactive iron to total iron ratios greater than 0.38, and most TOC to total sulfur ratios exceeding 2. These data indicate that the organic-rich shales of the Shahejie Formation were formed as a result of high primary productivity during the warm and humid middle Eocene period, coupled with the efficient preservation of organic matter in anoxic bottom waters. Negative δ13Corg and δ34Spy excursions recorded in the Shahejie Formation indicate water column conditions to have been influenced by transient volcanic eruptions. Positive δ13Corg and negative δ34Spy excursions may have been caused by hydrothermal fluids input whereas δ34Spy values approaching 20‰ suggest frequent marine transgressions. In particular, despite potential inputs of S into the paleolake by volcanism, hydrothermal fluids, or marine transgressions, bacterial sulfate reduction efficiently depleted the sulfate pool to have created ferruginous geochemistry water conditions for the effective preservation of organic carbon in sediments. Our results establish a direct link between lacustrine shale geochemical signatures and geological phenomena that impact its sedimentation.
Suggested Reviewers:	Jun Shen, Dr. Prof., China Univerisity of Geology （Wuhan） shenjun@cug.edu.cn Prof. Shen is a global environmentalist with a broad perspective, he published several papers in Nature Communications about volcanism
	Mingyu Zhao, Dr. Associate Prof., CAS Institute of Geology and Geophysics mingyu.zhao@mail.iggcas.ac.cn Dr. Zhao made a big progress in the sphere interaction and nutrient circulation, some of the papers are published in Nature Geoscience.

	Zhengbing Wang, Dr. Delft University of Technology Zheng.Wang@wldelft.nl Prof. Wang has made great progress in the ecological environment research of estuarine delta and near coastal zones.
	Qiyuan Sun, Dr. Fujian Normal University minglei_2008@fjnu.edu.cn Dr. Sun does research on the formation of organic matter in rivers and lakes for more than 10 years, and can give the comments from a morden perspective.
	Meng Cheng, Dr. Chengdu University of Technology mengcheng@cdut.edu.cn Dr. Cheng knows a lot about the carbon and sulfur cycles in oceans and lakes.
	Jian Cao, Dr. Nanjing University jcao@nju.edu.cn
	Xiting Liu, Dr. Ocean University of China liuxiting@ouc.edu.cn former reviewer
Response to Reviewers:	

Dear Editor Wei Ouyang,

We gratefully acknowledge the reviewer's positive evaluation of our work and agree with the comments of the second reviewer. We appreciate the editor's help in improving the manuscript, as well as the editorial support and suggestions. According to the proposed comments, we carefully revised the manuscript. The responses to the comments of the second reviewer are listed point-by-point in the attached file "Response to reviewers", the revisions are annotated red through the manuscript (in the version of track changes). The manuscript is co-authored by Sergei Katsev, Quanyou Liu, Gleb S. Pokrovski and Zhijun Jin. We kindly ask you to consider it for publication in *"Science of the Total Environment"*.

In the revised manuscript, we used total organic carbon content, iron speciation, organic carbon isotope ($\delta^{13}C_{org}$), and pyrite sulfur isotope ($\delta^{34}S_{py}$) data to establish relationships between organic carbon preservation and anoxic conditions in fine-grained sediments from the middle Eocene lacustrine depositional environments of the Jiyang Depression, Bohai Bay Basin, eastern China. Our results identified that despite potential inputs of S into the paleolake by volcanism, hydrothermal fluids, or transgression, bacterial sulfate reduction depleted the sulfate pool sufficiently to have created ferruginous geochemistry water conditions for the effectively preservation of organic carbon in sediments of Shahejie Formation. This is a direct link between lacustrine organic carbon burial and its controlling factors among multivariate geological events.

We believe that the revised manuscript will be of interest to the readership of researchers and professionals working on lacustrine environments. This manuscript has not been published or presented elsewhere in part or in entirety and is not under consideration by another journal. We have read and understood your journal's policies, and we believe that neither the manuscript nor the study violates any of these. There are no conflicts of interest to declare.

Thank you very much for your time and consideration. I look forward to hearing from you.

Sincerely,

Xinping Liang
Institute of Energy, Peking University, Beijing, 100871, China;
xinping.liang@pku.edu.cn

Carbon, iron and sulfur record of lacustrine paleo-environments during the middle Eocene in eastern China

Xinping Liang[a,c], Sergei Katsev[b], Quanyou Liu[a*], Gleb S. Pokrovski[c], Zhijun Jin[a,d*]

a. State Key Laboratory of Shale Oil and Gas Enrichment Mechanisms and Effective Development, Institute of Energy, Peking University, Beijing 100871, China;

b. Large Lakes Observatory and Department of Physics, University of Minnesota Duluth, 2205 E 5th St, Duluth, MN 55812, USA;

c. Géosciences Environnement Toulouse, Université Toulouse III – Paul Sabatier, CNRS, IRD, CNES, OMP, 14 avenue Edouard Belin, F-31400 Toulouse, France;

d. Sinopec Petroleum Exploration and Production Research Institute, Beijing, 100083, China

*Corresponding author: liuqy@pku.edu.cn or qyouliu@sohu.com (QY.L.) and jinzj1957@pku.edu.cn (Z.J.J)

Dear Editor Wei Ouyang and dear reviewers,

We gratefully appreciate your help in improving the manuscript, as well as the editorial support and suggestions. Thank you for the positive evaluation of our work and we agree with the minor revisions. According to the proposed constructive comments, we carefully revised the manuscript and needed figures. The revisions are annotated red through the manuscript in the version of track changes. The manuscript is co-authored by Xinping Liang, Sergei Katsev, Quanyou Liu, Gleb S. Pokrovski and Zhijun Jin. We kindly ask you to consider it for publication in *"Science of the Total Environment"*.

1. Followed by the editor's suggestions, we submitted:

1) Cover Letter;
2) revised manuscript with changes marked red;
3) revised manuscript with no changes marked;
4) Graphical Abstract;
5) Figures and Tables as separate files (Table 1 as separate file in Word format);
6) 3 points of Highlights (maximum 85 characters, including spaces, per bullet point);
7) response to Reviewers point-by-point;

and we REMOVED the original version of our submission.

2. Here are the responses to the comments of Reviewer #2.

Comments:

After reviewing the manuscript, I recommend minor revisions before acceptance.

The carbon isotopes of organic matter and the sulfur isotopes of pyrite are influenced by sedimentary environment evolution and sediment dynamics, which should be considered.

The iron speciation is affected by the sedimentary environment and redox conditions, with the contents of ferrous carbonate and pyrite competing with each other. I suggest the authors consider some modern sedimentary environment studies to enhance their discussion of the marine transgression in the study area. Relevant references for consideration include: Liu et al., 2023, SB; Zhang et al., 2024, 3P; Kong et al., 2024, MG; Zhang et al., CG, 2024.

Response:

We are grateful for this kind suggestion and the references. We agree with the reviewer's point that the influencing factors of carbon isotopes of organic matter ($\delta^{13}C_{org}$), the sulfur isotopes of pyrite ($\delta^{34}S_{py}$) and the iron speciation should be considered when these indicators are applied in the interpretation of paleoenvironments. As our samples are all fine-grained sediments in the semi-deep to deep lake, the TOC values vary between 1% and 10% (average 4%), and in the detailed core observations of the FY1 well, no strong storms, floods or fragments of higher plants were observed over a total length of 403.6 m, so we considered there was very few the terrestrial occasional effect, and the $\delta^{13}C_{org}$ and $\delta^{34}S_{py}$ could be used for most cases. Here we did not use the high C/S ratios to distinguish between marine and terrestrial sediments here because the sulfur content increasing can also be caused by volcanic or hydrothermal activities, neither does the pyrite content.

We agree with the reviewer's comment that the iron speciation is applied to interpret the sedimentary environment and redox conditions. Here as our magnetite content (Fe_{mag}) is low (< 0.13%), pointing to the absence of intense diagenetic transformation, so the iron speciation can be used to constrain the redox conditions of Shahejie Formation. As the oxidized Fe (Feox) is low, with

a maximum of 0.4%, so the contents of ferrous carbonate and pyrite compete with each other. This conclusion is also consistent with Liu et al.'s (2023, SB) viewpoint (Fig1.A, B). The difference between the samples of the two study areas is their total content, the total contents of ferrous carbonate and pyrite is lower than ~2% and ~6% respectively (Fig1.C), indicating the ferruginous to euxinic water conditions during Shahejie Formation.

As the TOC and $\delta^{13}C_{org}$ values shows different sources of organic matter (Fig1.D) between ECMZ core of modern sedimentary environment (Kong et al., 2024, 3P) and FY-1 Well core of Shahejie Formation, we compared the values of highly reactive iron between 91 samples of ECMZ core and 66 samples of FY-1 Well core of Shahejie Formation, to try to enhance the discussion of the marine transgression during middle Eocene (Fig1.E, F). Here in core ECMZ, authigenic minerals such as framboid pyrite aggregates can document the seawater intrusion in East China Sea, and continuous and slight decrease in the contents of magnetite and haematite illustrates that the sea level continued to rise (Liu et al., 2023, SB). However, this could happen after volcanic and hydrothermal activities during Shahejie Formation in Jiyang Lake. For example, as volcanic activity brings large amounts of nutrients and trace metals to the surface water, the positive feedback can increase paleoproductivity, accelerate the reducing bottom water conditions, and formed the high content of authigenic minerals such as framboid pyrite.

Therefore, we combined $\delta^{13}C_{org}$ to distinguish volcanism and transgressions because volcanism can cause negative $\delta^{13}C_{org}$ excursions, whereas marine transgressions usually happen in warmer climates and cause positive $\delta^{13}C_{org}$ excursions. Also, we propose that the precipitation of calcium carbonate in organic-rich shale is the result of increased pH due to strong photosynthesis by algae in the warm climate during marine transgression in the Jiyang calcareous lake. This may also be the difference between shallow marine and terrestrial deposits. Our mineral analyses show that the carbonate content in the study interval was generally high, with average calcite and dolomite contents of 37% and 10%, respectively. For example, the content of Fe_{carb} is higher than that of Fe_{py} from 3225 to 3200 m (Unit 5 in Fig.2), indicating that the sulfur isotope fractionation of pyrite in the paralic lakes during the sulfate reduction process was constrained by changes in the global sea level. The sea level increased in the warm and humid climate, brought large amounts of Ca^{2+} to form carbonates as well as high paleo-productivity promoted the deposition of organic-rich layers simultaneity. Thus formed the alternating carbonate and organic-rich shale layers, and after that the organic matter was degraded in a limited manner under ferruginous conditions and was well preserved. Saturated carbonate ions combined with iron and formed siderite, making its content higher in lacustrine sediments than that in modern sedimentary environments (Fig1.E).

This enhanced discussion of the marine transgression of the above explanation has been added in the manuscript. Please see lines *447-464*.

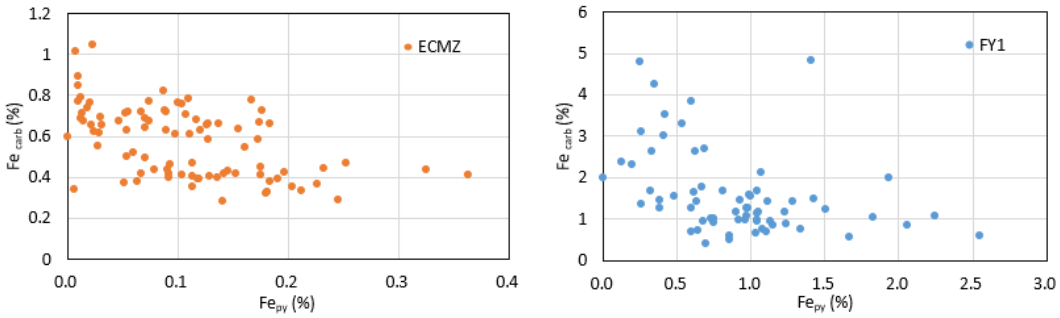

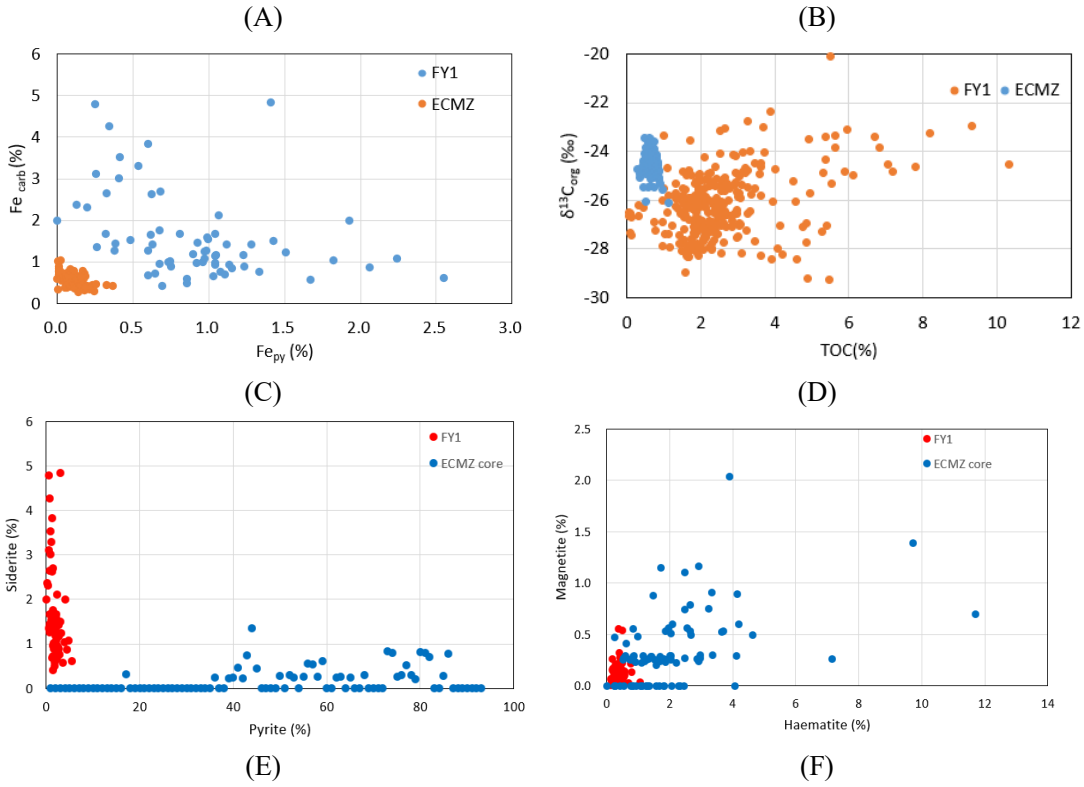

Fig.1. Comparison of the highly reactive iron values, TOC and $\delta^{13}C_{org}$ between samples of CEMZ core from modern sedimentary environment (Liu et al., 2023, SB; Zhang et al., 2024, 3P) and samples of FY1 Well from Jiyang Lake.

Thank you for your time and consideration. I look forward to hearing from you.

Best wishes for the journal "Science of the Total Environment"!

Yours sincerely,

Xinping Liang on behalf of all authors

xinping.liang@pku.edu.cn

Institute of Energy, Peking University

Carbon, iron and sulfur records of lacustrine paleo-environments during the middle Eocene in eastern China

Abstract

It is widely recognized that anoxic conditions facilitate the preservation of organic carbon in marine sediments. However, the specific geological factors that lead to the development of such conditions in paleo-lakes are less well understood. Owing to their smaller size, paleolakes could experience more frequent and stronger changes in geochemical conditions than oceans. Such changes, such as volcanism, hydrothermal fluids, or ocean transgressions, can also strongly affect the lacustrine organic carbon burial thereby complicating sediment diagenesis record. Here, we used total organic carbon content (TOC), organic carbon isotope ($\delta^{13}C_{org}$), iron speciation, and pyrite sulfur isotope ($\delta^{34}S_{py}$) data to establish relationships between organic carbon preservation and anoxic conditions in fine-grained sediments from the middle Eocene lacustrine depositional environments from the Shahejie Formation of the Jiyang Depression, Bohai Bay Basin, eastern China. The results reveal TOC between 1% and 10%, highly-reactive iron to total iron ratios greater than 0.38, and most TOC to total sulfur ratios exceeding 2. These data indicate that the organic-rich shales of the Shahejie Formation were formed as a result of high primary productivity during the warm and humid middle Eocene period, coupled with the efficient preservation of organic matter in anoxic bottom waters. Negative $\delta^{13}C_{org}$ and $\delta^{34}S_{py}$ excursions recorded in the Shahejie Formation indicate water column conditions to have been influenced by transient volcanic eruptions. Positive $\delta^{13}C_{org}$ and negative $\delta^{34}S_{py}$

excursions may have been caused by hydrothermal fluids input whereas $\delta^{34}S_{py}$ values approaching 20‰ suggest frequent marine transgressions. In particular, despite potential inputs of S into the paleolake by volcanism, hydrothermal fluids, or marine transgressions, bacterial sulfate reduction efficiently depleted the sulfate pool to have created ferruginous geochemistry water conditions for the effective preservation of organic carbon in sediments. Our results establish a direct link between lacustrine shale geochemical signatures and geological phenomena that impact its sedimentation.

Key words: organic carbon burial; ferruginous conditions; volcanism; transgression; paralic lacustrine shale; middle Eocene

1. Introduction

Anoxic conditions facilitate burial and preservation of organic carbon by slowing down microbial degradation, primarily in marine sediments (Shen Y. et al., 2003; Planavsky et al., 2011; Clarkson et al., 2014, 2016; Guilbaud et al., 2015; Raiswell et al., 2018), whilst factors that cause such conditions in lakes have not been sufficiently investigated. Multiple geologic events, such as volcanism, subsurface hydrothermal activity, and marine water incursion, can substantially affect sediment diagenesis and the burial of organic matter in both marine and lacustrine basins. Volcanic ash layers, for example, are prevalent in organic-rich deposits (organic carbon content greater than 2.0%) such as the Bazhenov Formation (western Siberia, Russia), the Eagle Ford Formation (Gulf Coast Basin, USA), the Wufeng-Longmaxi Formation (Sichuan Basin, China), the Fengcheng and Lucaogou Formations (Junggar Basin, China) (Ruebsam et

al., 2020; Liang et al., 2020; Liu et al., 2021, 2024). Volcanic activity may increase biological productivity in the photic zone by supplying nutrients and affect aquatic environments and their sedimentary records by providing fluxes of heat, dissolved carbon dioxide, and methane (Duggen et al., 2010; Langmann et al., 2010; Liu et al., 2019). Enhanced preservation of organic material in sediments can lead to the formation of organic-rich shales (Kim et al., 2015; LaRowe et al., 2020). Hydrothermal and volcanic inputs, recorded by high concentrations of metals and heterogeneous tuff in shales, are correlated with changes in paleo-productivity, anoxia, and organic matter burial (Magnall et al., 2016; He et al., 2020). However, the mechanisms by which geological events affect formation and preservation of organic matter in lacustrine environments are much less constrained than in marine environments.

Like the modern counterparts, ancient lakes were important sinks of organic carbon (Sklarew, 1979; Layton-Matthews et al., 2013; Swanner et al., 2020). Being much smaller than oceans, lakes are more sensitive to environmental changes and can record geologic events on shorter time scales. Paralic lakes, in particular, can be affected by volcanic activity, hydrothermal discharges, marine transgressions or other geological events (Malumián and Ramos, 1984; Duggen et al., 2010; Lee et al., 2018; Zeng et al., 2018; Zhang et al., 2018; Liu et al., 2024), so the controlling factors for the burial of lacustrine organic carbon are more complicated. For example, the Kabuno Bay (East Africa) is ferruginous, whereas Lake Kivu is sulfidic even though they both receive iron through hydrothermal sub-lacustrine springs (Bhattarai et al., 2012; Ross et al., 2014; Swanner et al. 2020). Studying variations in lacustrine conditions of sedimentation may help understand the analogous marine processes on their

correspondingly longer time scales.

In this regard, ancient lakes of the Jiyang Depression (Fig.1) in the Bohai Bay Basin, eastern China offer an excellent natural environment to investigate in detail the continental sedimentary record of the middle Eocene. A series of successive lacustrine shale sediments 150–300 m thick were deposited between the upper sub-member of Member 4 and the lower sub-member of Member 3 of the Shahejie Formation (Es_4^1 and Es_3^3) (Chen et al., 2008; Liang C. et al., 2018; Shi et al., 2019). This depositional period corresponds to a global increase in the atmospheric CO_2 during the Middle Eocene Climate Warming (MECO) (Fig.1, A; Lourens et al., 2005; Jovane et al., 2007; Zachos et al., 2008; Bijl et al., 2010). Therefore, this study combines total organic carbon contents (TOC) and total sulfur (TS) values of the Fanye-1 well (FY1, Fig. 1, B), with the vertical variation in Fe speciation, organic carbon isotope ($\delta^{13}C_{org}$), and pyrite sulfur isotope ($\delta^{34}S_{py}$) data, to establish a direct link between organic carbon preservation and anoxic conditions, and the factors that affect organic carbon burial in lacustrine basins during middle Eocene.

2. Geological Setting

The Bohai Bay Basin is a large Cenozoic sedimentary basin, which was formed at the intersection of three major tectonic regions that included the ancient Asian, Tethys and Pacific Oceans (Fig. 1, B). The subduction of the West Pacific plate under the North China Craton was the controlling factor in the tectonic evolution rate and orientation of the Bohai Bay Basin (Chen et al., 2008). Between the Late Paleocene and Eocene, subduction of the Pacific Plate decreased to its lowest rate of about 40

mm/a at 43 Ma, and the orientation changed from north-north-west to north-west-west. The rate gradually increased to 60 mm/a from 43 to 32 Ma, making the entire Asia continent an extended tectonic domain. This spreading reached its faulting limit at about 23 Ma in the Oligocene leading to the formation of the Late Mesozoic-Paleogene Bohai Bay Basin, which is divided into seven depressions and three uplifts (Chen et al., 2008).

Among them, the Jiyang Depression is the largest sedimentation center of the basin, spanning latitudes from 35 to 40°N. The depression is about 200 km long from east to west and 120 km wide from north to south, with a total area of 26,000 km^2 (Song et al., 2020). Cenozoic deposition during Es_4^1 and Es_3^3 sub-members in the Bohai Bay Basin coincided with an intensive fault depression, resulting in the formation of the Jiyang Lake whose estimated ancient depth was 190–290 m (Fig. 1., C) with the deepest area likely reaching 600 m (Chen et al., 2008). The lake has existed in the basin for about 4 million years and was connected to the west Pacific paleo-ocean during multiple periods, lasting for several thousand years each (Song et al., 2020). Between these episodes, the lake basin likely remained closed (Chen et al., 2008).

During Es_4^1 time, as the basin subsided, the lake experienced high salinities affected by different geological processes. During the Es_3^3 period of humid climate, as the lake basin widened and subsidence increased, the lake connected to the ocean, thus increasing accommodation space. Abundant semi-deep to deep waters (10–60 m depth) provided favorable conditions for deposition of fine-grained sedimentary rocks such as black shale. The rocks were predominantly argilitic with extensive layers of both massive and lamellar textures and with veins of sparry limestone, limy mudstone, and

dolomite (Chen et al., 2008; Liang C. et al., 2018; Song et al., 2020).

3. Materials and Methods

Core analysis shows that the high-quality source rocks of Es_4^1 and Es_3^3 (to ~1000 m) were widely distributed in semi-deep or deep lacustrine facies, intercalated with mm-to-cm think layers of volcanic ash in Jiyang Depression. Here a length of 403.6 m of whole-core was taken from the FY1 well (Shi et al., 2019; Song et al., 2020). Black and gray-black, layered, grainy, muddy shale dominates the Es_4^1 and Es_3^3 lithologies. A total of 270 core samples was obtained at a spacing of 1.0–1.5 m and these were analyzed for TOC, TS, $\delta^{13}C_{org}$ and major element analyses. A subset of 70 samples at an interval of 5–6 m was subjected to iron speciation and $\delta^{34}S_{py}$ analyses.

The concentrations of TOC and TS were determined using an Eltra infrared (IR) C/S analyzer from the discrepancy between the total carbon (or sulfur) determined by combustion and the total inorganic carbon (or sulfur) determined by acidification. Ultrapure 6 N HCl was added in a silver cup to dissolve inorganic carbon and sulfur (mostly carbonate and sulfide minerals) from weighed portions of powdered samples. Analyses of $\delta^{13}C_{org}$ were performed using a Costech™ 4010 coupled with a Thermo Finnigan MAT 253 via an open-split interface Conflo IV, with a reproducibility better than ±0.1‰ as based on the international standard IAEA-600 (caffeine, $\delta^{13}C_{org}$ = -27.77‰).

For major element concentrations (Fe, Al), 300 mg of powdered samples were burnt at 600 °C for 12 h in a muffle furnace to remove volatiles compounds, followed by a standard multi-acid (HF-HCl-HNO_3) digestion protocol designed for dissolution

in a Teflon bomb. An Agilent 7700 inductively coupled plasma mass spectrometer (ICP-MS) was used for the solution analyses, with an analytical precision of better than ± 5% (1σ) established using USGS standards (BHVO-2 and BCR-2).

Iron speciation and pyrite sulfur isotope analyses (in terms of $\delta^{34}S_{py}$) were performed for a total of 70 samples at the State Key Laboratory of Biogeology and Environmental Geology, China University of Geosciences (Wuhan). Iron as pyrite (Fe_{py}) was extracted using the chromium reduction method and iron speciation was determined by the sequential extraction method (Poulton and Canfield, 2005). Sulfur in pyrite (S_{py}) was extracted as H_2S using a hot $CrCl_2$ distillation for 2 h, trapped as silver sulfide (Ag_2S), which was then quantified gravimetrically. The Fe_{py} content in each sample was then calculated assuming the ideal pyrite stoichiometry (FeS_2). Iron from carbonate minerals (Fe_{carb}) was extracted by dissolution for 24 h in cold 10 wt% HCl. Then ferric Fe (oxyhydroxides, Fe_{ox}) was liberated from the residue of each sample, treated for 2 h with a sodium dithionite solution (50 g/L) buffered to a pH of ~5 with acetic acid and sodium citrate. Finally, Fe bound in magnetite (Fe_{mag}) was extracted for 6 h using a 0.2 M ammonium oxalate and 0.17 M oxalic acid solution (pH ~3). After diluting the extracts by a factor of 100 in 2 wt% HNO_3 (suprapure), an Agilent 7500ce ICP-MS was used to analyze each sequential extract. To increase precision, samples underwent processing in conjunction with internal calibration standards and blanks, by analyzing in duplicate each 10^{th} sample per batch. The analytical precision was better than 5% of the value.

Sulfur isotope ratios ($^{34}S/^{32}S$) were determined using a Thermo Fisher Scientific Delta V Plus isotope-ratio mass spectrometer coupled with a flash EA. The results are

expressed as $\delta^{34}S_{py}$ following the standard delta notation as per mil deviations relative to the Vienna Cañon Diablo Troilite (Li et al., 2021). An analytical uncertainty of 0.2‰ (1σ) for pyrite $\delta^{34}S$ was determined from replicate analyses of the International Atomic Energy Agency (IAEA) standards: S1 ($\delta^{34}S$ = -0.3‰), IAEA S2 ($\delta^{34}S$ = +22.65‰), and IAEA S3 ($\delta^{34}S$ = -32.5‰).

4. Results

The results of geochemical analyses of FY1 section are summarized in Table 1. The variation in chemical and isotopic composition of TOC, $\delta^{13}C_{org}$, TS, $\delta^{34}S_{py}$ and Fe redox as a function of depth is presented in Fig. 2. The study interval was divided into 7 units according to the changes in $\delta^{13}C_{org}$ and $\delta^{34}S_{py}$ values.

4.1. Organic carbon systematics

TOC values of the 270 samples vary from about 1 to 10 % with an average value close to 4%, and with maximum enrichment in Units 1 and 5 (Fig. 2), but without systematic differences between Es_3^3 and Es_4^1. The $\delta^{13}C_{org}$ values for samples of Es_4^1 vary within a relatively narrow range of about -29‰ to -20‰ with an average of ~ -26‰, whereas those from Es_3^3 vary within even narrower range of about -28‰ to -23‰ with a mean value -26‰ (Table 1). Samples with positive excursions of $\delta^{13}C_{org}$ values (> -24‰) are more frequent in Es_4^1, and are characterized by elevated TOC contents (> 4%). Samples showing more negative $\delta^{13}C_{org}$ (≤ -26‰) are also predominantly found in the Es_4^1 sub-member (Fig. 2A, B).

4.2. Iron systematics

In the lacustrine samples of Es_4^1 and Es_3^4, Fe_T values range between 1.4 and 8.0%, with an average close to 3% and are generally dominated by highly reactive iron (Fe_{HR}, including pyrite and carbonate iron, oxidized and magnetite iron) fraction (> 90% of Fe_T on average). Pyrite iron (Fe_{py}) ranges from 0.1 to 4% with an average of ~1%, which is slightly less than or comparable to carbonate iron (Fe_{carb}) content varying from 0.5 to 4 (average 1.5%). Oxidized iron (Fe_{ox}) is low, with a maximum of 0.4%. The Fe/Al ratios are systematically higher than 0.44 (with a single sample exception of 0.18 at 3346.9 m). Magnetite content (Fe_{mag}) is low (< 0.13%), pointing to the absence of digenesis; as a result, the iron speciation can be used to constrain the redox conditions. All Fe_{HR}/Fe_T values exceed 0.38, and almost all Fe_{py}/Fe_{HR} ratios are lower than 0.6, which is mostly due to the relatively high Fe_{carb} content.

Iron speciation is a widely used proxy for water column redox conditions, and can differentiate between oxic and anoxic (ferruginous or euxinic) environments (Poulton and Canfield, 2005, 2011). For anoxic conditions, Fe_{py}/Fe_{HR} ratios are used to distinguish ferruginous (typically < 0.7) and euxinic (typically > 0.8) conditions; however, more recent work suggested values above 0.6 as evidence of euxinia (Poulton, 2021). Under anoxic conditions, either diagenetic transformation of Fe_{HR} minerals into Fe-rich clay, or the swift sedimentation of deposits lacking iron, can lower Fe_{HR} concentrations. Total Fe/Al ratios provide complementary information on water column redox conditions. Indeed, although oxidative weathering or digenesis of samples could obscure Fe_{py} systematics, it would not significantly alter the Fe/Al ratios that are systematically lower than 0.44 in oxic marine sediments (Lyons and Severmann, 2006; Clarkson et al., 2014, 2016; Raiswell et al., 2018). Therefore, the

208 Fe/Al proxy in carbonate-rich sediments is relatively robust, provided Fe_T > 0.5 wt%
209 (Raiswell et al., 2018). For Fe_T < 0.5 wt%, carbonate samples have a greater potential
210 to be enriched in Fe_{HR} due to processes other than water column processes that arise
211 under anoxic conditions (e.g., post sedimentary diagenesis).

212 Overall, TOC values higher than 0.5%, with total iron > 0.5 wt%, Fe_{HR}/Fe_T ratios >
213 0.38 and Fe_{HR}/Fe_T ratios < 0.8 throughout the succession (Fig. 2, A, E, F) collectively
214 demonstrate predominantly anoxic ferruginous during the depositional period, despite
215 evidence of pyrite enrichment of considerable spatial and temporal variability that
216 cannot exclude local intermittent euxinic conditions in the basin.

217

218 **4.3. Sulfur systematics**

219 Total sulfur (TS) concentrations vary from about 0.2 to 11%, with an average of
220 ~1.4% across the two main intervals (Table 1, Fig. 2). Most samples (231) have
221 TOC/TS weight ratios above 2, with only a few (36) having TOC/TS < 2 (Fig. 2A, C).
222 According to Berner and Raiswell's (1984) analysis of modern sediments, TOC/TS
223 values of < 2 would correspond to euxinic conditions, those between 2 and 3.6
224 represent "normal" marine conditions, those of 3.6 to 10 reflect freshwater and
225 seawater transition zones, and those > 10 correspond to freshwater sediments.
226 Therefore, most of our samples from the study interval would indicate freshwater or
227 marine transitional conditions, with only rare instances of euxinia (Fig.3).

228 Values of $\delta^{34}S_{py}$ exhibit large variations within the studied section (Fig. 2D),
229 ranging from 9‰ to 36‰ with an average of ~ 20‰ with no significant differences
230 between Es_3^3 and Es_4^1 (Table 1). As sulfur isotope values in marine sulfates were ~ 22 ‰

during middle Eocene (Payton et al., 1998) and elevated $\delta^{34}S_{py}$ values (> 20‰) are consistent with the low levels of sulfate in the euxinic water column (Shen et al., 2003), our large $\delta^{34}S_{py}$ variations (Fig. 2D) indicate that redox conditions fluctuated considerably over time. However, despite the large environmental fluctuations in Jiyang Lake during the middle Eocene, fine-grained sediments were formed during the early stage of diagenesis in a closed system and were almost unaffected by late digenesis, which was consistent with very limited influence of weathering and metamorphism that could affect such sediments (Liang C. et al., 2018). This viewpoint is supported by the fact that interbedded carbonates and mudstones have consistently yielded similar redox interpretations across all instances of rock samples (Raiswell et al., 2018). Generally, the unusually high dolomite content in fine-grained sediments should indicate rather atypical lacustrine chemistry due to volcanism, hydrothermal fluids, or transgressions that may affected variability in calcium carbonate saturation leading to dolomite rather than calcite precipitation (Zhang et al., 2018; Liu et al., 2021).

5. Discussion

5.1. High primary productivity in middle Eocene warmhouse

Compared to the unmineralized fraction in deep sediments of modern large lakes and marine sediments (Galazzo et al., 2013; Liu et al., 2019, 2021), our high TOC values (average 4%) may indicate that the primary productivity of the lake over the entire interval (Es_4^1 to Es_3^3) was indeed higher than that during other MECO intervals (1−3% TOC; Galazzo et al., 2013). Algae-rich sediments worldwide are well-known to be a product of high primary productivity (Meyers, 1997). In Jiyang paleolakes,

algae-rich sedimentary layers, formed by alternating blooms of coccolithophytes and dinoflagellates, were a major feature of the Paleogene oil source rocks in the Bohai Bay Basin for more than 1 Ma (Xie et al., 2016; Song et al., 2020; Shi et al., 2021). These algal blooms are well recognized in the middle Eocene warming period of the Cenozoic (Bijl et al., 2010; Zachos et al., 2008; Pearson, 2010), which occurred 41.4−39.2 Ma ago (Shi et al., 2019). During this time, a warm climate and associated high productivity were favorable for oxygen consumption beneath the photic zone. The water column became anoxic, thereby leading to enhanced preservation and burial of organic matter. High productivity can be supported by systematically elevated concentrations of both TOC and barium (Zeng et al., 2018). TOC values above 6% are recorded here over 11 intervals across the depth range 3343.47 to 3102.67 m, with two intervals having TOC values as high as 8.4% and 10.4% at 3176.51 m and 3192.90 m, respectively (Fig.2). The average Ba concentrations in Es_4^1 and Es_3^3 are 470 and 560 ppm, respectively. Over the entire section in the Jiyang Depression, Ba values in samples positively correlate with the corresponding TOC values (Supplementary Table 2). For comparison, in a similar high paleoproductivity Lake Malawi (East Africa), the TOC concentrations are ~ 6 % in the sediments from the anoxic deep parts of the lake (Li et al., 2018).

Meanwhile, high primary productivity can also be confirmed by organic carbon isotope values. Most samples show $\delta^{13}C_{org}$ values between -29‰ and -25‰, indicating a source of lacustrine organic matter from exogenous terrestrial plants, authigenic phytoplankton photosynthesis, as well as possible allochthones (Meyers, 1997). Terrestrial C4 plants were very rare in the Jiyang Depression during the middle Eocene

277 as they are usually found in dry environments and have the $\delta^{13}C_{org}$ values higher than
278 -20‰. However, there might have been some C3 plants in the lake, because small
279 fragments of higher plants (including leaves) can be windblown and floating debris
280 could sink, although some of the compounds of terrestrial origin may have been
281 subsequently degraded by diagenesis. In the detailed core observations of the FY1 well,
282 over a total length of 403.6 m, no fragments of higher plants were observed. Generally,
283 there is no direct relationship between the concentration of biomarkers and the source
284 of organic matter because many biomarkers can be detected at very low concentrations.
285 There was probably some retene, oleanene, or β-carotene (Xu et al., 2020); however,
286 the contribution of higher plants to the preserved organic matter is expected to be small.
287 For another, the relative content of the biomarkers may also change further with
288 diagenesis. For example, Xu et al. (2020) also proposed an existing algae source of
289 retene, oleanene, or β-carotene during organic-rich shale formation. To sum up, the
290 contribution of organic matter of terrestrial origin from higher plants depends on the
291 lake size and sedimentation process. In a very large paralic lake continental runoff input
292 can be significant only due to strong storms, floods or other events from land. As there
293 were no land events in the Jiyang Depression with a total area of 26,000 km^2, the
294 detected compounds of higher plants do not mean that the terrestrial organic input is
295 significant in this offshore lake.

296 Combined with the sedimentary characteristics of modern lakes, we propose that
297 in the center of the paralic Jiyang lake like FY-1 Well, the organic matter may mainly
298 come from lacustrine authigenesis, the input of terrigenous organic matter, such as
299 plants, may only have occurred in brief periods. Of the studied 270 samples, only a few

(25 in Es_3^3 and 27 in Es_4^1) showed $\delta^{13}C_{org}$ values above -25‰, with an average TOC of 5% (Fig.2), indicating that during this period organic matter may have been occasionally derived from very limited amount of terrestrial plants. Thus, most of the organic matter enrichment in the source rocks of the Shahejie Formation likely resulted from native algal and bacterial production coupled with favorable preservation conditions. Due to a globally significant increase of greenhouse gases in the MECO atmosphere (Bijl et al., 2010), photosynthetic carbon fixation could lead to carbon isotope ratios as low as −29‰ (Hodell and Schelske, 1998). Therefore, we propose that the negative excursions of $\delta^{13}C_{org}$ corresponded to high primary productivity during warm and humid climate caused by periods of elevated atmospheric pCO_2. Under these elevated pCO_2, CO_2 was predominantly transported into lacustrine systems via photosynthesis, and was reduced by biological processes into organic matter with enrichment in the lighter isotope (^{12}C), thereby yielding negative excursions of $\delta^{13}C$ values.

5.2. Ferruginous/euxinic water conditions

Lallier-Verges et al. (1993) quantified the degree of bacterial sulfate reduction (BSR) using the sulfate reduction index (SRI), which is defined as the ratio of primary organic carbon to residual organic carbon. Primary organic carbon encompasses both the organic carbon depleted via sulfate reduction, and the residual total organic carbon (TOC (wt.%) at present). Organic carbon loss (C_{loss}) by degradation coupled with sulfate reduction may be assessed from the stoichiometry of the sulfate reduction equation proposed by Berner and Raiswell (1984):

$$SRI = (TOC + C_{loss})/TOC \quad (1)$$

$$\text{where } C_{loss} = TS/1.33 \quad (2)$$

Substituting (2) into (1) yields:

$$SRI = (TOC + TS/1.33)/TOC = 1 + 0.75 \times TS/TOC \quad (3)$$

The SRI is regarded as the lowest degradation consumption index for total organic carbon. The higher the BSR activity, the higher the SRI value, and the greater the organic matter consumption. For SRI < 1.375, the BSR intensity can be limited by total sulfate and the amount of undegraded TOC may increase substantially. For SRI > 1.375, the BSR intensity increases, and the overall TOC value is relatively low (Liu et al., 2021). The relationship between the sulfate reduction strength and the organic carbon content (SRI/TOC) in the study interval shows that most of the SRI values in the ferruginous water column are less than 1.375 (Fig. 4 (D)), indicating a weak sulfate reduction, which may have been conductive to organic matter preservation and burial. In contrast, euxinic waters with strong BSR may result both in organic preservation and consumption. It can be seen in Fig. 3 and 4 (D) that in the euxinic zone, most samples with TOC < 2 % have SRI values > 1.375.

Several mechanisms may have created ferruginous conditions at the bottom of the Jiyang lake. A combination of volcanism, hydrothermal fluids, and transgression may have brought reactive iron and maintained anoxic conditions, while the primary productivity was high. For example, volcanism could have increased nutrient influxes (Liu et al., 2019, 2024), and productivity, and stimulated oxygen consumption below the photic zone. Meanwhile, the isotopically “light” sulfur ($\delta^{34}S_{py}$ of 0 ‰) from a volcanic source was preferentially utilized by BSR, resulting in low $\delta^{34}S_{py}$ values.

However, intermittent sulfidization events in a ferruginous Jiyang Lake may not have led to elevated Fe_{py}/Fe_{HR} ratios compared to typical marine values of 0.7, because such an increase may be obscured by the high carbonate (Fe_{carb}) content largely dominating over Fe_{py} (Fig. 2, Unit 2, 3, 5). For all the samples, there are only two Fe_{py}/Fe_{HR} values above 0.7, with the corresponding $\delta^{34}S_{py}$ values of 24−25‰) (Fig. 4 A, C). The two $\delta^{34}S_{py}$ values, higher than those in the lower adjacent interval (~13 ‰), indicate that the basin became relatively closed and euxinic after a period of volcanism or hydrothermal activity. The positive $\delta^{34}S_{py}$ values (> 20‰) are higher than the sulfate ^{34}S from seawater during middle Eocene, indicating the depletion of the light sulfur isotopes in sulfate under strong BSR. Meanwhile, the TOC values for these two samples are 3.4 and 2.8% at 3332.39 and 3226.24 m, respectively (Fig. 2), which are less than the average value (4.0%) of the study interval, indicating that BSR consumed the primary organic matter and converted sulfate to H_2S, and promoted pyrite formation. A rough positive covariation between the Fe_{py}/Fe_{HR} ratios and TOC also supports the BSR occurrence (Fig. 4 A, B). However, the high TOC/TS ratios (> 2.0) and low sulfate reduction index (SRI) (< 1.375) suggest that it was sulfate availability, rather than organic matter supply, that constrained BSR in deep waters (Fig. 4 (D)).

For Jiyang Lake, there may have been occasional euxinic conditions as the TOC/TS values are less than 2 (in 36 samples from 270). Euxinia in the photic zone (from biomarker data) and deeper water (based on framboid size distributions) has been identified in Silurian, Devonian, Permian and Eocene oceans (Racka et al., 2010; Marynowski et al., 2012; Liu et al., 2019; Xu et al., 2020; Percival et al., 2022). Euxinia is prevalent in anoxic marine environments where sulfate is abundant. Modern

meromictic lakes develop euxinia when sulfate concentrations exceed 100 μM, while below that threshold their monimolimnia (the deep stagnant layers) tend to be ferruginous. Xu et al. (2020) demonstrated that there were different euxinic water conditions during the deposition of the Shahejie Formation, evidenced by variations in the aryl isoprenoid ratio, relative amount of isorenieratane, long-chain n-alkane carbon isotopic composition and other molecular indicators, which indicated different intensity of bacterial sulfate reaction (BSR). In Jiyang Lake, potential sources for extra sulfate could have been episodic (for 5−10 ka) marine transgressions (Unit 2 and Unit 5), volcanism (Unit 1, 2, 3 of Es_4^1, and Unit 5 of Es_3^3) or hydrothermal fluids (Unit 4 of Es_3^3) (Fig. 2). Outside these episodes, sulfate would become depleted by BSR, Fe_{py}/Fe_{HR} values were mostly < 0.6 and Fe_{HR}/Fe_T values > 0.38 (Fig.4 A), which also suggests that the deep-water column throughout the middle Eocene was predominantly ferruginous. Meanwhile, there might also be very occasional oxic episodes identified by the presence of bioturbation in anoxic brackish water (Song et al., 2020). Although Fe shuttling could potentially create local enrichments of Fe_{carb} (Fig.4 (B)) or Fe_{ox}, resulting in high Fe_{HR}/Fe_T and low Fe_{py}/Fe_{HR} ratios, the deep lake was probably anoxic and ferruginous during most of the depositional period. The reduced Fe transported from the anoxic water column could have led to Fe_{carb} enrichments in bioturbated sediments. As anoxic ferruginous conditions expanded and contracted over time, reactive iron enrichment could form in even deeper settings.

In summary, the Fe_{HR} values between 1.2% and 6.6% generally show the same evolution trend as the total of Fe_{py} and Fe_{carb}, while Fe_{ox} and Fe_{mag} have little correlation with the Fe_{HR} content trend. Thus, organic matter enrichment was primarily created by

both enhanced preservation under ferruginous water conditions and high paleo-productivity with limited dilution of the shale by terrigenous clastic materials (Xie et al., 2016; Song et al., 2020).

5.3. Impacts of geological events on organic carbon burial

Our core analyses demonstrate that volcanism, hydrothermal activity, and marine transgressions affected the study area. Only few investigations of carbon and pyrite sulfur isotopic variations focused on lacustrine sedimentary intervals during the MECO. Our study uses different covariations between $\delta^{34}S_{py}$ and $\delta^{13}C_{org}$ values (Fig. 2B, D) to establish a relationship between geological events, biological productivity, and water redox conditions. It has been shown that a negative excursion of 2 to 6‰ in $\delta^{13}C_{org}$ of both carbonate and organic carbon is linked to global volcanism (Lee et al., 2018; Liu et al., 2019; Longman et al., 2019; Shen J. et al., 2019b; Li Y. et al., 2021). Indeed, in the study intervals, volcanism effects are evident in nine prominent negative excursions in $\delta^{13}C_{org}$ (Fig. 2B), which are correlated with tuff interlayers (Fig. 5). The pyroclastic interlayers in the shales are predominantly vitreous and crystalline debris of andesite (Fig. 5 (C, D)), in which microfractures were developed and ostracod fragments were deposited. Such negative excursions in $\delta^{13}C_{org}$ values are typically associated with increases in primary productivity, which can be brought about by the increased delivery of nutrients following the volcanic events.

The same layers with highly negative $\delta^{13}C_{org}$ are also associated with negative shifts in $\delta^{34}S_{py}$ (as low as 8.9‰; Fig. 2D). The water column in the deep lake was usually closed when there were no geological events. In this case, the SO_4^{2-} reservoir is limited and could not be replenished. With the continuing exhaustion of the sulfate

reservoir (enriched in ^{34}S) by sulfur reduction through dissimilation, $^{34}S_{py}$ gradually increased and approached that of the initial sulfate. In contrast to open marine sediments, $^{34}S_{py}$ values in an almost infinite sea water sulfate reservoir, are usually below 0‰ (Li et al., 2021). Volcanic and hydrothermal activity generate sulfur with $\delta^{34}S$ of 0 to 5‰ (Huston, 1999), which is substantially below the values of water surface-sourced sulfate (~ 20‰ during study period). If sub-lacustrine eruptions of a volcano or associated geothermal fluids carried $H_2{}^{32}S$-enriched sulfide sulfur into a closed lake, its reaction with highly reactive iron could form isotopically equivalent $Fe^{32}S_2$-enriched pyrite within a quite short period of time (i.e. several years). This process caused the decrease in $\delta^{34}S_{py}$ values along with the sulfate of the light sulfur isotope was consumed by BSR. As volcanic $H_2{}^{32}S$ was quickly consumed by iron and the BSR began to reduce sulfate in a closed system, the resulting pyrite had lighter $\delta^{34}S$ values. Higher $\delta^{34}S_{py}$ values then formed again at low sulfate concentrations at the end of sulfate reduction. If volcanic activities or deep fluids carried large amounts of oxidized volatiles, such as SO_2, BSR would have been enhanced and more ^{32}S consumed. As a result, $^{34}S_{py}$ first decreased and then increased with an increased amount of sulfate consumption. Indeed, this trend could be identified especially in Units 1 and 3 of Es_4^1 (Fig. 2D). Because the bottom waters of the paleolake seemed to have remained ferruginous, the iron input (as Fe (II); Isley and Abbott, 1999; Kump and Seyfried, 2005) during these volcanic or hydrothermal activities must have exceeded the inputs of sulfur into the lake.

The presence of marine ostracods (Fig 5 (A)), elevated $\delta^{34}S_{py}$ values (~20 ‰) and high carbonate content (Fe_{carb} to ~5%) collectively indicate marine transgressions,

which is consistent with the interpretation of the strata using the method of astronomical cycles (Ma et al., 2023). During middle Eocene warming, marine transgressions increased the lake water depth and supplied ^{34}S-enriched sulfate, causing the $\delta^{34}S_{py}$ value of pyrite to approach that of seawater. The $\delta^{34}S_{py}$ values vary between 9 and 36 ‰, being both lower and higher than those of the marine sulfates identified during the MECO (20.9 ± 0.5‰; Longinelli, 1989; Kampschulte et al., 2001). Marine transgressions may have occurred roughly every 1,000 years over a period of 5,000 years (Fig. 2, Units 2 and 5). As BSR generates isotopically light sulfide, the heavier $\delta^{34}S_{py}$ values can be attributed to the consumption of sulfate sulfur after staged transgression when the lake system closed again. Mineral analyses show that the total content of Fe_{mag} and Fe_{ox} is low, with a maximum of 0.37%, so the contents of ferrous carbonate and pyrite compete with each other. This is consistent with most sediments in modern paralic environment (Liu et al., 2023; Zhang et al., 2024). Only the difference between the samples of the two study areas is the contents of ferrous carbonate, indicating the different water conditions during their sediment deposition. In Shahejie Formation, the carbonate content in the study interval was generally high, with average calcite and dolomite contents of 37% and 10%, respectively. For example, the content of Fe_{carb} is higher than that of Fe_{py} from 3225 to 3200 m in Unit 5 (Fig.2), indicating that the sulfur isotope fractionation of pyrite in the paralic lakes during the sulfate reduction process was constrained by changes in the global sea level. The sea level increased in the warm and humid climate, and transgression brought large amounts of Ca^{2+} to form carbonates. Meanwhile, high paleo-productivity also promoted the deposition of organic-rich layers. Therefore, the precipitation of calcium

carbonate and organic matter layers is the result of increased pH due to strong photosynthesis by algae in the warm climate during marine transgressions in the Jiyang calcareous lake. After that, the organic matter was degraded in a limited manner under ferruginous conditions and was well preserved.

The delicate equilibrium between ferruginous and euxinic chemical conditions could be influenced by the comparable rates of Fe_{HR} and sulfate input fluxes. On a global scale, continental sources stand out as the primary contributors to the potential Fe_{HR} flux. At the regional scale, geological events, such as volcanic activity or ocean transgression, could also have liberated some reactive iron and sulfate into the lake, providing a conceivable mechanism for the transportation of ferrous iron and resulting in a disproportionate increase in the Fe_{HR} flux relative to that of sulfate. The interplay of all these processes have generated dominantly ferruginous environments during the middle Eocene in the Jiyang Depression.

On the basis of the aforementioned research, we propose that there was an extensive burial of lacustrine organic carbon in Eastern China during the warm and humid climate of the middle Eocene, which thereby created a positive feedback loop in the Earth's climate system. Frequent volcanic activity during the early stages of Es_4^1 might have brought aerosols to increase the albedo in the short-term cold climate (Fig.6B, maybe to 10 years). Most importantly, it released abundant CO_2 into in the atmosphere and brought reactive iron and nutrients to create optimal environments for the growth and expansion of algae and plankton in the later stages (Fig.6A, to 1 million years) of the middle Eocene. As temperatures increased, the biological productivity in Jiyang Lake increased, leading to enhanced production of total organic carbon in

ferruginous water conditions. This positive feedback mechanism may have contributed to the sustained warmth of the middle Eocene climate. Based on this analysis, we highlight a combined effect on sedimentation of external events such as input of volcanic ash, intermittent hydrothermal fluids and marine transgressions during middle Eocene continental warming of western Pacific. These events could not only supply nutrients and catalytic elements to promote biological productivity and cause oxygen consumption, but they also enhanced the reactive iron input to form the dynamic anoxic ferruginous conditions that were conducive for the preservation of organic carbon.

6. Conclusions

The widespread terrestrial sedimentary and geochemical records of the middle Eocene in the Eastern China have been established using novel TOC, TS, iron speciation, $\delta^{13}C_{org}$ and $\delta^{34}S_{py}$ data. These data, including the highly-reactive iron to total iron ratios ($Fe_{HR}/Fe_T > 0.38$), along with a wide range of total organic carbon content (TOC, from 1 to 10 %) exceeding that of total sulfur (TOC/TS > 2), and low sulfate reduction indexes (SRI < 1.375), collectively suggest widespread anoxic and ferruginous conditions that would have been favorable for burial of lacustrine organic carbon during the middle Eocene in the paralic lacustrine environments of the Jiyang Depression. The temporal stability of lacustrine ferruginous water conditions may have been due to the warm and humid climate during the middle Eocene, with high biological productivity and large oxygen consumption in the water column, leading to efficient burial of organic carbon in deep sediments.

Both $\delta^{13}C_{org}$ and $\delta^{34}S_{py}$ values reveal transient geological events such as volcanism,

hydrothermal fluids, and transgressions. Negative $\delta^{13}C_{org}$ and $\delta^{34}S_{py}$ excursions along the sedimentary column point to transient volcanic events, whereas positive $\delta^{13}C_{org}$ along with negative $\delta^{34}S_{py}$ excursions indicate injection of associated hydrothermal fluids; in contrast, elevated $\delta^{34}S_{py}$ (to ~20‰) point to frequent marine transgressions. Despite potential inputs of sulfur into the paleolake as a result of these geological events, bacterial sulfate reduction efficiently consumed the sulfate pool, thereby creating ferruginous water conditions favorable for the efficient preservation of organic carbon.

Acknowledgments

We thank Yunqing Hao for assistance with microscopic slice analyses and for discussions, Prof. Chao Li and Prof. Yan'an Shen for help with the geochemical analyses, Prof. Bing Shen and Dr. Huiyuan Xu for discussions. This work was supported by the National Natural Science Foundation of China (Grants 42172151, 41811530094, and 41625009), the China Postdoctoral Science Foundation (Grant 2021M690204), and the National Key Research and Development Program (Grant 2023YFF0806200). We thank the two reviewers and the editorial support for the constructive comments, which have greatly improved the quality of this paper.

Research Data

All of the processed data discussed has been uploaded in the supplementary tables.

References

Berner, R. A., Raiswell, R.,1984. C/S method for distinguishing freshwater from marine sedimentary

rocks. Geology 12 (6), 365–368. DOI: 10.1130/0091-7613(1984)12<365:CMFDFF>2.0.CO;2
Bhattarai, S., Ross, K.A., Schmid, M., Anselmetti, F.S., Bürgmann, H., 2012. Local Conditions Structure Unique Archaeal Communities in the Anoxic Sediments of Meromictic Lake Kivu. Microb. Ecol. 64 (2), 291–310. DOI: 10.1007/s00248-012-0034-x
Bijl, P.K., Houben, A.J.P., Schouten, S., Bohaty, S.M., Sluijs, A., Reichart, G.J., Sinninghe D.J., Brinkhuis, H., 2010. Transient middle Eocene atmospheric CO_2 and temperature variations. Science 330 (6005), 819–821. DOI: 10.1126/science.1193654
Clarkson, M.O., Poulton, S.W., Guilbaud, R., Wood, R., 2014. Assessing the utility of Fe/Al and Fe-speciation to record water column redox conditions in carbonate-rich sediments. Chem. Geol. 382, 111–122. DOI: 10.1016/j.chemgeo.2014.05.031
Clarkson, M.O., Wood, R.A., Poulton, S.W., Richoz, S., Newton, R.J., Kasemann, Bowyer, F., Krystyn, L., 2016. Dynamic anoxic ferruginous conditions during the end-Permian mass extinction and recovery. Nat. Commun. 7, 12236. DOI: 10.1038/ncomms12236
Duggen, S., Olgun, N., Croot, P., Hoffmann, L., Dietze, H., Teschner, C., 2010. The role of airborne volcanic ash for the surface ocean biogeochemical iron-cycle: a review. Biogeosciences 7, 827–844. DOI: 10.5194/bgd-6-6441-2009
Galazzo, B.F, Giusberti, L, Luciani, V, Thomas, E., 2013. Paleoenvironmental changes during the Middle Eocene Climatic Optimum (MECO) and its aftermath: The benthic foraminiferal record from the Alano section (NE Italy). Palaeogeogr. Palaeoclimatol. Palaeoecol. 378, 22–35. DOI: 10.1016/j.palaeo.2013.03.018
Guilbaud, R., Poulton, S.W., Butterfield, N.J., Zhu, M., Shields-Zhou, G.A., 2015. A global transition to ferruginous conditions in the early Neoproterozoic oceans. Nat. Geosci. 8(6), 1–5. DOI: 10.1038/ngeo2434
He, R., Lu, W., Junium, C.K., Straeten, C.A.V., Lu, Z., 2020. Paleo-redox context of the Mid-Devonian Appalachian Basin and its relevance to biocrises. Geochim. Cosmochim. Acta 287, 328–340. DOI: 10.1016/j.gca.2019.12.019
Hodell, D.A., Schelske, C.L., 1998. Production, sedimentation, and isotopic composition of organic matter in Lake Ontario. Limnol. Oceanogr. 43, 200–214. https://doi.org/10.4319/lo.1998.43.2.0200
Huston., David L., 1997. Stable Isotopes and Their Significance for Understanding the Genesis of Volcanic-Hosted Massive Sulfide Deposits: A Review. Volcanic Associated Massive Sulfide Deposits: Processes and Examples in Modern and Ancient Settings, C. Tucker Barrie, Mark D. Hannington. https://doi.org/10.5382/Rev.08.07
Isley, A.E., Abbott, D.H., 1999. Plume-related mafic volcanism and the deposition of banded iron formation. J. Geophys. Res.: Solid Earth. 104 (B7), 15461–15477. https://doi.org/10.1029/1999JB900066
Jovane, L., Florindo, F., Coccioni, R., Dinarès-Turell, J., Marsili A., Monechi, S., Roberts, A., Sprovieri, M., 2007. The middle Eocene climatic optimum event in the Contessa Highway section, Umbrian Apennines, Italy. GSA Bull. 119 (3-4), 413–427. DOI: 10.1130/B25917.1
Kampschulte, A., Bruckschen, P., Strauss, H., 2001. The Sulphur isotopic composition of trace sulphates in Carboniferous brachiopods: implications for coeval seawater, correlation with other geochemical cycles and isotope stratigraphy. Chem. Geol., 175 (1), 149-173. DOI: 10.1016/S0009-2541(00)00367-3
Kim, T.Y., North, R.L., Guildford, S.J., Dillon, P., Smith, R.E.H., 2015. Phytoplankton productivity and size composition in Lake Simcoe: The nearshore shunt and the importance of autumnal production. J. Great Lakes Res. 41 (4), 1075–1086. https://doi.org/10.1016/j.jglr.2015.09.011

Kump, L. R., Seyfried, W. E., 2005. Hydrothermal Fe fluxes during the Precambrian: effect of low oceanic sulfate concentrations and low hydrostatic pressure on the composition of black smokers. Earth Planet. Sci. Lett. 235, 654–662. DOI: 10.1016/j.epsl.2005.04.040

Lallier-Verges, E., Bertrand, P., Desprairies, A., 1993. Organic matter composition and sulfate reduction intensity in Oman Margin sediments. Mar. Geol., 112, 57–69. DOI: 10.1016/0025-3227(93)90161-N

Langmann, B., Zaksek, K., Hort, M., Duggen S., 2010. Volcanic ash as fertiliser for the surface ocean. Atmos. Chem. Phys. 10, 3891–3899. DOI: 10.5194/acp-10-3891-2010

LaRowe, D.E., Arndt, S., Bradley, J.A., Estes, E.R., Hoarfrost, A., Lang, S.Q., Lloyd, K.G., Mahmoudi, N., Orsi, W.D., Shah, W.S.R., Steen. A.D., Zhao. R., 2020. The fate of organic carbon in marine sediments - New insights from recent data and analysis. Earth Sci. Rev. 204, 103146. DOI: 10.1016/j.earscirev.2020.103146

Layton-Matthews, D., Leybourne, M.I., Peter, J.M., Scott, S.D., Cousens, B., Eglington, B.M., 2013. Multiple sources of selenium in ancient seafloor hydrothermal systems: Compositional and Se, S, and Pb isotopic evidence from volcanic-hosted and volcanic-sediment-hosted massive sulfide deposits of the Finlayson Lake District, Yukon, Canada. Geochim. Cosmochim. Acta 117, 313–331. DOI: 10.1016/j.gca.2013.05.002

Lee, C-T.A., Jiang, H., Ronay, E., Minisini, D., Stiles, J., Neal, M., 2018. Volcanic ash as a driver of enhanced organic carbon burial in the Cretaceous. Sci. Rep. 8, 4197. DOI: 10.1038/s41598-018-22576-3

Li, J., Brown, E.T., Crowe, S.A., Katsev, S., 2018. Sediment geochemistry and contributions to carbon and nutrient cycling in a deep meromictic tropical lake: Lake Malawi (East Africa). J. Great Lakes Res. 44: 1221–1234. https://doi.org/10.1016/j.jglr.2017.12.001

Li, Y., Zhang, T., Shen, B., Li, Z., Shao, D., Lash, G.G., 2021. Carbon and sulfur isotope variations through the Upper Ordovician and Lower Silurian of South China linked to volcanism. Palaeogeogr. Palaeoclimatol. Palaeoecol. 567, 110285. DOI: 10.1016/j.palaeo.2021.110285

Liang, C., Jiang, Z.X., Cao, Y.C., Wu, J., Wang, Y.S., Hao, F., 2018, Sedimentary characteristics and origin of lacustrine organic-rich shales in the salinized Eocene Dongying Depression. GSA Bulletin 130 (1-2):154–174. DOI: 10.1130/B31584.1

Liang, J., Wang, H., Bai, Y., Ji, X., Duo, X., 2016. Cenozoic tectonic evolution of the Bohai Bay Basin and its coupling relationship with Pacific Plate subduction. J Asian Earth Sci 127, 257–266. http://dx.doi.org/10.1016/j.jseaes.2016.06.012

Liang, X., Jin Z., Philippov, V.P., Obryadchikov, O.S., Zhong, D., Liu, Q., Uspensky, B., Morozov, V., 2020. Sedimentary features of Domanik shelf carbonate measures during regression in the southeastern Volga-Ural basin. Mar. Petrol. Geol. 2020, 119, 104438. DOI: 10.1016/j.marpetgeo.2020.104438

Liu, Q, Zhu, D, Meng, Q, Liu, J, Wu, X, Zhou, B, Fu, Q, Jin, Z. 2019. The scientific connotation of oil and gas formations under deep fluids and organic-inorganic interaction. Sci. China Earth Sci. 62: 507–528. DOI: 10.1007/s11430-018-9281-2

Liu, Q., Li, P., Jin, Z., Liang, X., Zhu, D., Wu, X., Meng, Q., Liu, J., Fu, Q., Zhao, J., 2021. Preservation of organic matter in shale linked to bacterial sulfate reduction (BSR) and volcanic activity under marine and lacustrine depositional environments. Mar. Petro. Geol. 127, 2021,104950. DOI: 10.1016/j.marpetgeo.2021.104950

Liu, Q., Li, P., Jiang, L., Jin, Z., Liang, X., Zhu, D., Pang, Q., Zhang, R., Liu, J., 2024. Distinctive volcanic ash–rich lacustrine shale deposition related to chemical weathering intensity during the Late Triassic: Evidence from lithium contents and isotopes. Sci. Adv. 10 (11), 1–9. DOI:

10.1126/sciadv.adi6594
Liu, X., Hu, Y., Dong, J., Li, A., Zhuang, G., Wang, H., 2023. Iron-bearing minerals indicate sea-level rise of the East China Sea inner shelf since the last deglaciation. Sci. Bull. 68(4), 364–366. https://doi.org/10.1016/j.scib.2023.02.002
Longinelli, A., 1989. Oxygen-18 and sulphur-34 in dissolved oceanic sulphate and phosphate. In: Fritz, P., Fontes, J.C., (eds), Handbook of environmental isotope geochemistry, 3. Elsevier, Amsterdam, 221–255. Illustration, Table; ref: 7p, ISSN 0167-949X http://pascal-francis.inist.fr/vibad/index.php?action=getRecordDetail&idt=7227509
Longman, J., Palmer, M.R., Gernon, T.M., Manners, H.R., 2019. The role of tephra in enhancing organic carbon preservation in marine sediments. Earth Sci. Rev. 192, 480–490. DOI: 10.1016/j.earscirev.2019.03.018
Lourens, L.J., Sluijs, A., Kroon, D., Zachos, J.C., Thomas, E., Röhl, U., Bowles, J., Raffi, I., 2005. Astronomical pacing of late Palaeocene to early Eocene global warming events. Nature 435, 1083–1087. DOI: 10.1038/nature03814
Lyons, T.W., Severmann, S., 2006. A critical look at iron paleoredox proxies: New insights from modern euxinic marine basins. Geochim. Cosmochim. Acta 70, 5698–5722. DOI: 10.1016/j.gca.2006.08.021
Ma, Y, Fan, M., Li, M., Ogg, J., Zhang, C., Feng, J., Zhou, C., Liu, X., Lu, Y., Liu, H., Eldrett, J.S., Ma, C., 2023. East Asian lake hydrology modulated by global sea-level variations in the Eocene warmhouse. Earth Planet. Sci. Lett. 602, 117925. DOI: 10.1016/j.epsl.2022.117925
Magnall, J.M., Gleeson, S.A., Blamey, N.J.F., Paradis, S., Luo, Y., 2016. The thermal and chemical evolution of hydrothermal vent fluids in shale hosted massive sulphide (SHMS) systems from the MacMillan Pass district (Yukon, Canada). Geochim. Cosmochim. Acta 193, 251–273. DOI: 10.1016/j.gca.2016.07.020
Malumián, N., Ramos, V.A.,1984. Magmatic intervals, transgression-regression cycles and oceanic events in the Cretaceous and Tertiary of southern South America. Earth Planet. Sci. Lett., 67 (2), 228–237. DOI: 10.1016/0012-821X(84)90118-3
Marynowski, L., Zatoń, M., Rakociński, M., Filipiak, P., Kurkiewicz, S., Pearce, T.J., 2012. Deciphering the upper Famennian Hangenberg Black Shale depositional environments based on multi-proxy record. Palaeogeogr. Palaeoclimatol. Palaeoecol. 346-347, 66–86. DOI: 10.1016/j.palaeo.2012.05.020
Meyers, P.A., 1997. Organic geochemical proxies of paleoceanographic, paleolimnologic, and paleoclimatic processes. Org. Geochem. 27(5–6), 213–250. DOI: 10.1016/S0146-6380(97)00049-1
Paytan, A., M. Kastner, D., Campbell, M.H. Thiemens, 1998. Sulfur isotope composition of Cenozoic seawater sulfate. Science 282, 1459-1462.
Pearson P.N., 2010. Increased Atmospheric CO_2 During the Middle Eocene. Science Science 330 (6005), 763–4. DOI: 10.1126/science.1197894
Percival, L.M.E., Marynowski, L., Baudin, F., Goderis S., Vleeschouwer D. De, Rakociński M., Narkiewicz K., Corradini C., Silva A. C. Da, Claeys P., 2022. Combined Nitrogen-Isotope and Cyclostratigraphy Evidence for Temporal and Spatial Variability in Frasnian–Famennian Environmental Change. Geochem. Geophys. Geosys. 23(5), e2021GC010308 DOI: https://doi.org/10.1029/2021GC010308
Planavsky, N.J., McGoldrick, P., Scott, C.T., Li, C., Reinhard, C.T., Kelly, A.E., Chu, X., Bekker, A., Love, G.D., Lyons, T.W., 2011. Widespread iron-rich conditions in the mid-Proterozoic ocean. Nature 477, 448–451. DOI: 10.1038/nature10327

669 Ploeg, R.V.D., Cramwinckel, M. J., Kocken, I. J., Leutert, T. J., Bohaty, S. M., Fokkema, C. D., Hull,
670 P. M., Meckler, A. N., Middelburg, J. J., Müller, I. A., Penman, D. E., Peterse, F., Reichart, G.-
671 J., Sexton, P. F., Vahlenkamp M., Vleeschouwer, D. D., Wilson, P. A., Ziegler, M., Sluijs, A.,
672 2023. North Atlantic surface ocean warming and salinization in response to middle Eocene
673 greenhouse warming. Sci. Adv. 9, eabq0110. DOI: 10.1126/sciadv.abq0110
674 Poulton, S.W., Canfield, D.E., 2005. Development of a sequential extraction procedure for iron:
675 Implications for iron partitioning in continentally derived particulates. Chem. Geol. 214, 209–
676 221. DOI: 10.1016/j.chemgeo.2004.09.003
677 Poulton, S.W., Canfield, D.E., 2011. Ferruginous conditions: A dominant feature of the ocean through
678 Earth's history. Elements 7, 107–112. DOI: 10.2113/gselements.7.2.107
679 Poulton, S.W., 2021. The Iron Speciation Paleoredox Proxy: Elements in Geochemical Tracers in
680 Earth System Science: New York, Cambridge University Press, 24 p.
681 https://doi.org/10.1017/9781108847148.
682 Racka M., Marynowski L., Filipiak P., Sobstel M., Pisarzowska A., Bond D. P.G., 2010. Anoxic
683 Annulata Events in the Late Famennian of the Holy Cross Mountains (Southern Poland):
684 Geochemical and palaeontological record. Palaeogeogr. Palaeoclimatol. Palaeoecol. 297(3-4),
685 549–575. DOI: 10.1016/j.palaeo.2010.08.028
686 Raiswell, R., Hardisty, D.S., Lyons, T.W., Canfield, D.E., Owens, J.D., Planavsky, N.J., Poulton,
687 S.W., Reinhard, C.T.,2018. The iron paleoredox proxies: A guide to the pitfalls, problems and
688 proper practice. Am. J. Sci. 318 (5), 491–526. DOI: 10.2475/05.2018.03
689 Ross, K. A., Smets, B., Batist, M.D., Hilbe, M., Schmid, M., Anselmetti, F.S., 2014. Lake-level rise
690 in the late Pleistocene and active subaquatic volcanism since the Holocene in Lake Kivu, East
691 African Rift. Geomorphology, 221, 274–285. DOI: 10.1016/j.geomorph.2014.05.010
692 Ruebsam, W., Pieńkowski, G., Schwark, L., 2020. Toarcian climate and carbon cycle perturbations
693 – its impact on sea-level changes, enhanced mobilization and oxidation of fossil organic matter.
694 Earth Planet. Sci. Lett. 546, 116417. DOI: 10.1016/j.epsl.2020.116417
695 Shen, J., Yu, J.X., Chen, J.B., Algeo, T.X., Xu, G.Z., Feng, Q.L., Shi, X., Planavsky, N.J., Shu, W.C.,
696 Xie, S.C., 2019. Mercury evidence of intense volcanic effects on land during the Permian-
697 Triassic transition. Geology. 47, 1117–1121.
698 Shen, W., Shao, L., Zhou, Q., Liu, J., Eriksson, K.A., Kang, S. and Steel, R.J., 2024. The role of
699 fluvial and tidal currents on coal accumulation in a mixed-energy deltaic setting: Pinghu
700 Formation, Xihu Depression, East China Sea Shelf Basin. Sedimentology, 71: 173-206.
701 https://doi.org/10.1111/sed.13133
702 Shen, Y., Knoll, A.H., Walter, M.R., 2003. Evidence for low sulphate and anoxia in a mid-Proterozoic
703 marine basin. Nature 423, 632–635. DOI: 10.1038/nature01651
704 Shi, J., Jin, Z., Liu, Q., Zhang, R., Huang, Z., 2019. Cyclostratigraphy and astronomical tuning of the
705 middle Eocene terrestrial successions in the Bohai Bay Basin, Eastern China. Global Planet.
706 Change 174, 115–126. DOI: 10.1016/j.gloplacha.2019.01.001
707 Song, M., Liu, H., Wang, Y., Liu, Y., 2020. Enrichment rules and exploration practices of Paleogene
708 shale oil in Jiyang Depression, Bohai Bay Basin, China. Petrol. Explor. Develop. 47 (2), 242–
709 253. DOI: 10.1016/S1876-3804(20)60043-X
710 Swanner, E.D., Lambrecht, N., Wittkop, C., Harding, C., Katsev, S., Torgeson, J., Poulton, S.W.,
711 2020. The biogeochemistry of ferruginous lakes and past ferruginous oceans. Earth Sci. Rev.
712 211, 103430. DOI: 10.1016/j.earscirev.2020.103430
713 Xie, X., Li, M., Littke, R., Huang, Z., Ma, X., Jiang, Q., Snowdon L. R., 2016. Petrographic and
714 geochemical characterization of microfacies in a lacustrine shale oil system in the Dongying Sag,

715 Jiyang Depression, Bohai Bay Basin, eastern China. Int. J Coal Geol., 165, 49–63. DOI:
716 10.1016/j.coal.2016.07.004
717 Xu, H., Hou, D., Löhr, S.C., Liu, Q., George, S.C., 2020. Early diagenetic pyrite cementation
718 influences molecular composition of sedimentary organic matter in the Dongying Depression,
719 China. Org. Geochem., 144, 104019. DOI: 10.1016/j.orggeochem.2020.104019
720 Zachos J. C., Dickens Gerald R., Zeebe Richard E., 2008. An early Cenozoic perspective on
721 greenhouse warming and carbon-cycle dynamics. Science 451, 279–283. DOI:
722 10.1038/nature06588
723 Zeng, Z., Pike, M., Tice, M.M., Kelly, C., Marcantonio, F., Xu, G., Maulana, I., 2018, Iron
724 fertilization of primary productivity by volcanic ash in the Late Cretaceous (Cenomanian)
725 Western Interior Seaway. Geology 46, 859–862. DOI: 10.1130/G45304.1
726 Zhang, L., Wang, C., Wignall, P.B., Kluge, T., Gao, Y., 2018. Deccan volcanism caused coupled
727 pCO_2 and terrestrial temperature rises, and pre-impact extinctions in northern China. Geology
728 46 (3), 271–274. DOI: 10.1130/G39992.1
729 Zhang, M., Liu, X., Li, A., Chang, X., Hu, L., Bi., N., Zhuang. G., Wang, H., 2024. Fate of terrigenous
730 organic carbon within shelf sediments from the East China Sea controlled by sea-level and
731 climatic changes since the last deglaciation. Palaeogeogr. Palaeoclimatol. Palaeoecol. 650,
732 112386. https://doi.org/10.1016/j.palaeo.2024.112386

733

734 Table and Figure captions

735

736 Table 1. Summary data of total organic carbon (TOC), organic carbon isotope
737 composition ($\delta^{13}C_{org}$), total sulfur (TS), pyrite sulfur isotope ($\delta^{34}S_{py}$), Fe/Al ratio, and
738 iron speciation of samples in the FY1 Well (data range, arithmetic average and number
739 of samples, see Supplementary Table 1 for data points).

740

741 Figure 1. (A) Map of sites with existing MECO records on a paleogeographic
742 reconstruction for the middle Eocene at 40 Ma (modified from Ploeg et al., 2023). (B)
743 Simplified geological map of Bohai Bay Basin in western Pacific, showing the core
744 location of FY-1 Well in the Jiyang Depression in eastern China (modified from Liang
745 et al., 2016). (C) Stratigraphic column of the study interval in the middle Eocene. The
746 Es_4^1 and Es_3^3 sediments are deposited during the rifting stage over 38–50 Ma ago

747 (modified from Shi et al., 2019).

748

749 Figure 2. Iron speciation, $\delta^{13}C_{org}$, TOC, and $\delta^{34}S_{py}$ values as a function of depth from
750 the middle Eocene (Es_4^1–Es_3^3) black shales in the Jiyang Depression (geological
751 timescale from Shi et al., 2019). (A) total organic carbon (TOC), (B) $\delta^{13}C_{org}$, (C) total
752 sulfur content (TS), (D) pyrite sulfur isotope ($\delta^{34}S_{py}$), (E) ratio of highly reactive Fe
753 to total Fe (Fe_{HR}/Fe_T), (F) ratio of pyrite iron to highly reactive iron (Fe_{py}/Fe_{HR}), (G)
754 content of pyrite iron, (H) content of carbonate iron. Note that Fe_{HR} =
755 $Fe_{py}+Fe_{ox}+Fe_{mag}+Fe_{carb}$, the thresholds for oxic versus anoxic (0.22–0.38) and
756 ferruginous versus euxinic conditions (0.6–0.8) are from Poulton et al. (2021); the
757 units of the study interval are based on lithological and geochemical differences, as
758 discussed in the text.

759

760 Figure 3. Plots of TOC vs TS, showing that the salinity of the most samples was similar
761 to the salinity of seawater, corresponding to ferruginous water conditions.

762

763 Figure 4. Plots of (A) Fe_{HR}/Fe_T vs Fe_{py}/Fe_{HR}; (B) Fe_{carb} vs Fe_{py}; (C) Fe_{py}/Fe_{HR} vs $\delta^{34}S_{py}$;
764 (D) TOC vs SRI.

765

766 Figure 5. Microscopic features of volcanic ash in the Middle Eocene shale of the Jiyang
767 Depression. (A) ostracod fragments in shales; (B) interbedded tuffs and shale; (C)
768 interbedded tuffs and shale with micro fractures; (D) pyroclastic interlayer in shales.

769

770 Figure 6. Sedimentary model of the paralic lake basin in the Jiyang Depression

developed in this study. (A) High primary productivity during middle Eocene long-time warmth. (B) Impacts of different geological events on organic carbon burial. During a short period of cooling caused by volcanism, despite potential external sulfur inputs, bacterial sulfate reduction sufficiently depleted the sulfate pool to have created ferruginous conditions.

Graphical Abstract

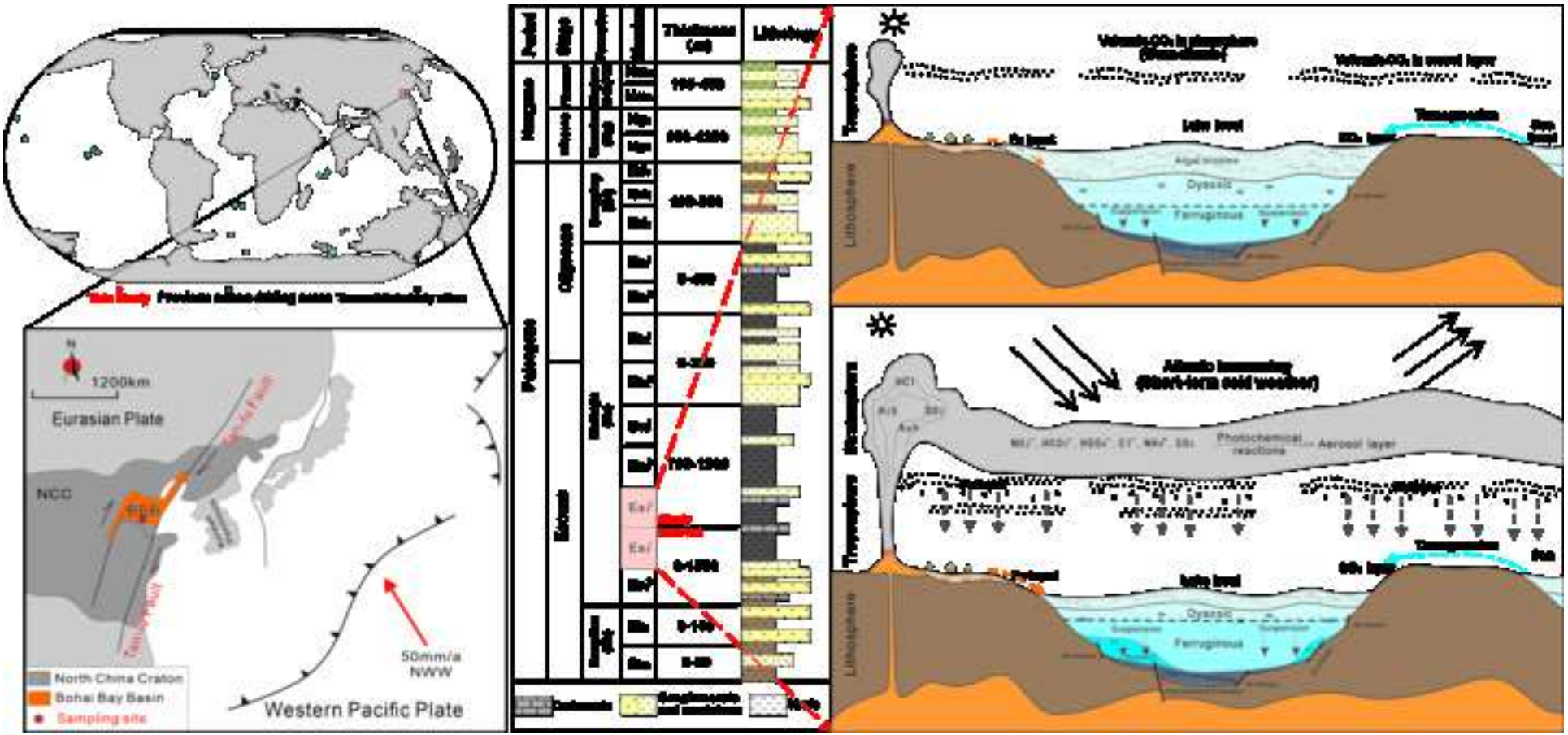

Highlights

- The primary productivity was high during the Shahejie Formation in middle Eocene.
- Ferruginous conditions were predominant during lacustrine OC preservation.
- Multivariate geological events enhanced OC burial in paralic paleoenvironments.

Carbon, iron and sulfur records of lacustrine paleo-environments during the middle Eocene in eastern China

Abstract

It is widely recognized that anoxic conditions facilitate the preservation of organic carbon in marine sediments. However, the specific geological factors that lead to the development of such conditions in paleo-lakes are less well understood. Owing to their smaller size, paleolakes could experience more frequent and stronger changes in geochemical conditions than oceans. Such changes, such as volcanism, hydrothermal fluids, or ocean transgressions, can also strongly affect the lacustrine organic carbon burial thereby complicating sediment diagenesis record. Here, we used total organic carbon content (TOC), organic carbon isotope ($\delta^{13}C_{org}$), iron speciation, and pyrite sulfur isotope ($\delta^{34}S_{py}$) data to establish relationships between organic carbon preservation and anoxic conditions in fine-grained sediments from the middle Eocene lacustrine depositional environments from the Shahejie Formation of the Jiyang Depression, Bohai Bay Basin, eastern China. The results reveal TOC between 1% and 10%, highly-reactive iron to total iron ratios greater than 0.38, and most TOC to total sulfur ratios exceeding 2. These data indicate that the organic-rich shales of the Shahejie Formation were formed as a result of high primary productivity during the warm and humid middle Eocene period, coupled with the efficient preservation of organic matter in anoxic bottom waters. Negative $\delta^{13}C_{org}$ and $\delta^{34}S_{py}$ excursions recorded in the Shahejie Formation indicate water column conditions to have been influenced by transient volcanic eruptions. Positive $\delta^{13}C_{org}$ and negative $\delta^{34}S_{py}$

excursions may have been caused by hydrothermal fluids input whereas $\delta^{34}S_{py}$ values approaching 20‰ suggest frequent marine transgressions. In particular, despite potential inputs of S into the paleolake by volcanism, hydrothermal fluids, or marine transgressions, bacterial sulfate reduction efficiently depleted the sulfate pool to have created ferruginous geochemistry water conditions for the effective preservation of organic carbon in sediments. Our results establish a direct link between lacustrine shale geochemical signatures and geological phenomena that impact its sedimentation.

Key words: organic carbon burial; ferruginous conditions; volcanism; transgression; paralic lacustrine shale; middle Eocene

1. Introduction

Anoxic conditions facilitate burial and preservation of organic carbon by slowing down microbial degradation, primarily in marine sediments (Shen Y. et al., 2003; Planavsky et al., 2011; Clarkson et al., 2014, 2016; Guilbaud et al., 2015; Raiswell et al., 2018), whilst factors that cause such conditions in lakes have not been sufficiently investigated. Multiple geologic events, such as volcanism, subsurface hydrothermal activity, and marine water incursion, can substantially affect sediment diagenesis and the burial of organic matter in both marine and lacustrine basins. Volcanic ash layers, for example, are prevalent in organic-rich deposits (organic carbon content greater than 2.0%) such as the Bazhenov Formation (western Siberia, Russia), the Eagle Ford Formation (Gulf Coast Basin, USA), the Wufeng-Longmaxi Formation (Sichuan Basin, China), the Fengcheng and Lucaogou Formations (Junggar Basin, China) (Ruebsam et

al., 2020; Liang et al., 2020; Liu et al., 2021, 2024). Volcanic activity may increase biological productivity in the photic zone by supplying nutrients and affect aquatic environments and their sedimentary records by providing fluxes of heat, dissolved carbon dioxide, and methane (Duggen et al., 2010; Langmann et al., 2010; Liu et al., 2019). Enhanced preservation of organic material in sediments can lead to the formation of organic-rich shales (Kim et al., 2015; LaRowe et al., 2020). Hydrothermal and volcanic inputs, recorded by high concentrations of metals and heterogeneous tuff in shales, are correlated with changes in paleo-productivity, anoxia, and organic matter burial (Magnall et al., 2016; He et al., 2020). However, the mechanisms by which geological events affect formation and preservation of organic matter in lacustrine environments are much less constrained than in marine environments.

Like the modern counterparts, ancient lakes were important sinks of organic carbon (Sklarew, 1979; Layton-Matthews et al., 2013; Swanner et al., 2020). Being much smaller than oceans, lakes are more sensitive to environmental changes and can record geologic events on shorter time scales. Paralic lakes, in particular, can be affected by volcanic activity, hydrothermal discharges, marine transgressions or other geological events (Malumián and Ramos, 1984; Duggen et al., 2010; Lee et al., 2018; Zeng et al., 2018; Zhang et al., 2018; Liu et al., 2024), so the controlling factors for the burial of lacustrine organic carbon are more complicated. For example, the Kabuno Bay (East Africa) is ferruginous, whereas Lake Kivu is sulfidic even though they both receive iron through hydrothermal sub-lacustrine springs (Bhattarai et al., 2012; Ross et al., 2014; Swanner et al. 2020). Studying variations in lacustrine conditions of sedimentation may help understand the analogous marine processes on their

correspondingly longer time scales.

In this regard, ancient lakes of the Jiyang Depression (Fig.1) in the Bohai Bay Basin, eastern China offer an excellent natural environment to investigate in detail the continental sedimentary record of the middle Eocene. A series of successive lacustrine shale sediments 150–300 m thick were deposited between the upper sub-member of Member 4 and the lower sub-member of Member 3 of the Shahejie Formation (Es_4^1 and Es_3^3) (Chen et al., 2008; Liang C. et al., 2018; Shi et al., 2019). This depositional period corresponds to a global increase in the atmospheric CO_2 during the Middle Eocene Climate Warming (MECO) (Fig.1, A; Lourens et al., 2005; Jovane et al., 2007; Zachos et al., 2008; Bijl et al., 2010). Therefore, this study combines total organic carbon contents (TOC) and total sulfur (TS) values of the Fanye-1 well (FY1, Fig. 1, B), with the vertical variation in Fe speciation, organic carbon isotope ($\delta^{13}C_{org}$), and pyrite sulfur isotope ($\delta^{34}S_{py}$) data, to establish a direct link between organic carbon preservation and anoxic conditions, and the factors that affect organic carbon burial in lacustrine basins during middle Eocene.

2. Geological Setting

The Bohai Bay Basin is a large Cenozoic sedimentary basin, which was formed at the intersection of three major tectonic regions that included the ancient Asian, Tethys and Pacific Oceans (Fig. 1, B). The subduction of the West Pacific plate under the North China Craton was the controlling factor in the tectonic evolution rate and orientation of the Bohai Bay Basin (Chen et al., 2008). Between the Late Paleocene and Eocene, subduction of the Pacific Plate decreased to its lowest rate of about 40

mm/a at 43 Ma, and the orientation changed from north-north-west to north-west-west. The rate gradually increased to 60 mm/a from 43 to 32 Ma, making the entire Asia continent an extended tectonic domain. This spreading reached its faulting limit at about 23 Ma in the Oligocene leading to the formation of the Late Mesozoic-Paleogene Bohai Bay Basin, which is divided into seven depressions and three uplifts (Chen et al., 2008).

Among them, the Jiyang Depression is the largest sedimentation center of the basin, spanning latitudes from 35 to 40°N. The depression is about 200 km long from east to west and 120 km wide from north to south, with a total area of 26,000 km^2 (Song et al., 2020). Cenozoic deposition during Es_4^1 and Es_3^3 sub-members in the Bohai Bay Basin coincided with an intensive fault depression, resulting in the formation of the Jiyang Lake whose estimated ancient depth was 190–290 m (Fig. 1., C) with the deepest area likely reaching 600 m (Chen et al., 2008). The lake has existed in the basin for about 4 million years and was connected to the west Pacific paleo-ocean during multiple periods, lasting for several thousand years each (Song et al., 2020). Between these episodes, the lake basin likely remained closed (Chen et al., 2008).

During Es_4^1 time, as the basin subsided, the lake experienced high salinities affected by different geological processes. During the Es_3^3 period of humid climate, as the lake basin widened and subsidence increased, the lake connected to the ocean, thus increasing accommodation space. Abundant semi-deep to deep waters (10–60 m depth) provided favorable conditions for deposition of fine-grained sedimentary rocks such as black shale. The rocks were predominantly argilitic with extensive layers of both massive and lamellar textures and with veins of sparry limestone, limy mudstone, and

dolomite (Chen et al., 2008; Liang C. et al., 2018; Song et al., 2020).

3. Materials and Methods

Core analysis shows that the high-quality source rocks of Es_4^1 and Es_3^3 (to ~1000 m) were widely distributed in semi-deep or deep lacustrine facies, intercalated with mm-to-cm think layers of volcanic ash in Jiyang Depression. Here a length of 403.6 m of whole-core was taken from the FY1 well (Shi et al., 2019; Song et al., 2020). Black and gray-black, layered, grainy, muddy shale dominates the Es_4^1 and Es_3^3 lithologies. A total of 270 core samples was obtained at a spacing of 1.0–1.5 m and these were analyzed for TOC, TS, $\delta^{13}C_{org}$ and major element analyses. A subset of 70 samples at an interval of 5–6 m was subjected to iron speciation and $\delta^{34}S_{py}$ analyses.

The concentrations of TOC and TS were determined using an Eltra infrared (IR) C/S analyzer from the discrepancy between the total carbon (or sulfur) determined by combustion and the total inorganic carbon (or sulfur) determined by acidification. Ultrapure 6 N HCl was added in a silver cup to dissolve inorganic carbon and sulfur (mostly carbonate and sulfide minerals) from weighed portions of powdered samples. Analyses of $\delta^{13}C_{org}$ were performed using a Costech™ 4010 coupled with a Thermo Finnigan MAT 253 via an open-split interface Conflo IV, with a reproducibility better than ±0.1‰ as based on the international standard IAEA-600 (caffeine, $\delta^{13}C_{org}$ = -27.77‰).

For major element concentrations (Fe, Al), 300 mg of powdered samples were burnt at 600 °C for 12 h in a muffle furnace to remove volatiles compounds, followed by a standard multi-acid (HF-HCl-HNO_3) digestion protocol designed for dissolution

in a Teflon bomb. An Agilent 7700 inductively coupled plasma mass spectrometer (ICP-MS) was used for the solution analyses, with an analytical precision of better than ± 5% (1σ) established using USGS standards (BHVO-2 and BCR-2).

Iron speciation and pyrite sulfur isotope analyses (in terms of $\delta^{34}S_{py}$) were performed for a total of 70 samples at the State Key Laboratory of Biogeology and Environmental Geology, China University of Geosciences (Wuhan). Iron as pyrite (Fe_{py}) was extracted using the chromium reduction method and iron speciation was determined by the sequential extraction method (Poulton and Canfield, 2005). Sulfur in pyrite (S_{py}) was extracted as H_2S using a hot $CrCl_2$ distillation for 2 h, trapped as silver sulfide (Ag_2S), which was then quantified gravimetrically. The Fe_{py} content in each sample was then calculated assuming the ideal pyrite stoichiometry (FeS_2). Iron from carbonate minerals (Fe_{carb}) was extracted by dissolution for 24 h in cold 10 wt% HCl. Then ferric Fe (oxyhydroxides, Fe_{ox}) was liberated from the residue of each sample, treated for 2 h with a sodium dithionite solution (50 g/L) buffered to a pH of ~5 with acetic acid and sodium citrate. Finally, Fe bound in magnetite (Fe_{mag}) was extracted for 6 h using a 0.2 M ammonium oxalate and 0.17 M oxalic acid solution (pH ~3). After diluting the extracts by a factor of 100 in 2 wt% HNO_3 (suprapure), an Agilent 7500ce ICP-MS was used to analyze each sequential extract. To increase precision, samples underwent processing in conjunction with internal calibration standards and blanks, by analyzing in duplicate each 10^{th} sample per batch. The analytical precision was better than 5% of the value.

Sulfur isotope ratios ($^{34}S/^{32}S$) were determined using a Thermo Fisher Scientific Delta V Plus isotope-ratio mass spectrometer coupled with a flash EA. The results are

expressed as $\delta^{34}S_{py}$ following the standard delta notation as per mil deviations relative to the Vienna Cañon Diablo Troilite (Li et al., 2021). An analytical uncertainty of 0.2‰ (1σ) for pyrite $\delta^{34}S$ was determined from replicate analyses of the International Atomic Energy Agency (IAEA) standards: S1 ($\delta^{34}S$ = -0.3‰), IAEA S2 ($\delta^{34}S$ = +22.65‰), and IAEA S3 ($\delta^{34}S$ = -32.5‰).

4. Results

The results of geochemical analyses of FY1 section are summarized in Table 1. The variation in chemical and isotopic composition of TOC, $\delta^{13}C_{org}$, TS, $\delta^{34}S_{py}$ and Fe redox as a function of depth is presented in Fig. 2. The study interval was divided into 7 units according to the changes in $\delta^{13}C_{org}$ and $\delta^{34}S_{py}$ values.

4.1. Organic carbon systematics

TOC values of the 270 samples vary from about 1 to 10 % with an average value close to 4%, and with maximum enrichment in Units 1 and 5 (Fig. 2), but without systematic differences between Es_3^3 and Es_4^1. The $\delta^{13}C_{org}$ values for samples of Es_4^1 vary within a relatively narrow range of about -29‰ to -20‰ with an average of ~ -26‰, whereas those from Es_3^3 vary within even narrower range of about -28‰ to -23‰ with a mean value -26‰ (Table 1). Samples with positive excursions of $\delta^{13}C_{org}$ values (> -24‰) are more frequent in Es_4^1, and are characterized by elevated TOC contents (> 4%). Samples showing more negative $\delta^{13}C_{org}$ (≤ -26‰) are also predominantly found in the Es_4^1 sub-member (Fig. 2A, B).

4.2. Iron systematics

In the lacustrine samples of Es_4^1 and Es_3^4, Fe_T values range between 1.4 and 8.0%, with an average close to 3% and are generally dominated by highly reactive iron (Fe_{HR}, including pyrite and carbonate iron, oxidized and magnetite iron) fraction (> 90% of Fe_T on average). Pyrite iron (Fe_{py}) ranges from 0.1 to 4% with an average of ~1%, which is slightly less than or comparable to carbonate iron (Fe_{carb}) content varying from 0.5 to 4 (average 1.5%). Oxidized iron (Fe_{ox}) is low, with a maximum of 0.4%. The Fe/Al ratios are systematically higher than 0.44 (with a single sample exception of 0.18 at 3346.9 m). Magnetite content (Fe_{mag}) is low (< 0.13%), pointing to the absence of digenesis; as a result, the iron speciation can be used to constrain the redox conditions. All Fe_{HR}/Fe_T values exceed 0.38, and almost all Fe_{py}/Fe_{HR} ratios are lower than 0.6, which is mostly due to the relatively high Fe_{carb} content.

Iron speciation is a widely used proxy for water column redox conditions, and can differentiate between oxic and anoxic (ferruginous or euxinic) environments (Poulton and Canfield, 2005, 2011). For anoxic conditions, Fe_{py}/Fe_{HR} ratios are used to distinguish ferruginous (typically < 0.7) and euxinic (typically > 0.8) conditions; however, more recent work suggested values above 0.6 as evidence of euxinia (Poulton, 2021). Under anoxic conditions, either diagenetic transformation of Fe_{HR} minerals into Fe-rich clay, or the swift sedimentation of deposits lacking iron, can lower Fe_{HR} concentrations. Total Fe/Al ratios provide complementary information on water column redox conditions. Indeed, although oxidative weathering or digenesis of samples could obscure Fe_{py} systematics, it would not significantly alter the Fe/Al ratios that are systematically lower than 0.44 in oxic marine sediments (Lyons and Severmann, 2006; Clarkson et al., 2014, 2016; Raiswell et al., 2018). Therefore, the

Fe/Al proxy in carbonate-rich sediments is relatively robust, provided Fe_T > 0.5 wt% (Raiswell et al., 2018). For Fe_T < 0.5 wt%, carbonate samples have a greater potential to be enriched in Fe_{HR} due to processes other than water column processes that arise under anoxic conditions (e.g., post sedimentary diagenesis).

Overall, TOC values higher than 0.5%, with total iron > 0.5 wt%, Fe_{HR}/Fe_T ratios > 0.38 and Fe_{HR}/Fe_T ratios < 0.8 throughout the succession (Fig. 2, A, E, F) collectively demonstrate predominantly anoxic ferruginous during the depositional period, despite evidence of pyrite enrichment of considerable spatial and temporal variability that cannot exclude local intermittent euxinic conditions in the basin.

4.3. Sulfur systematics

Total sulfur (TS) concentrations vary from about 0.2 to 11%, with an average of ~1.4% across the two main intervals (Table 1, Fig. 2). Most samples (231) have TOC/TS weight ratios above 2, with only a few (36) having TOC/TS < 2 (Fig. 2A, C). According to Berner and Raiswell's (1984) analysis of modern sediments, TOC/TS values of < 2 would correspond to euxinic conditions, those between 2 and 3.6 represent "normal" marine conditions, those of 3.6 to 10 reflect freshwater and seawater transition zones, and those > 10 correspond to freshwater sediments. Therefore, most of our samples from the study interval would indicate freshwater or marine transitional conditions, with only rare instances of euxinia (Fig.3).

Values of $\delta^{34}S_{py}$ exhibit large variations within the studied section (Fig. 2D), ranging from 9‰ to 36‰ with an average of ~ 20‰ with no significant differences between Es_3^3 and Es_4^1 (Table 1). As sulfur isotope values in marine sulfates were ~ 22 ‰

during middle Eocene (Payton et al., 1998) and elevated $\delta^{34}S_{py}$ values (> 20‰) are consistent with the low levels of sulfate in the euxinic water column (Shen et al., 2003), our large $\delta^{34}S_{py}$ variations (Fig. 2D) indicate that redox conditions fluctuated considerably over time. However, despite the large environmental fluctuations in Jiyang Lake during the middle Eocene, fine-grained sediments were formed during the early stage of diagenesis in a closed system and were almost unaffected by late digenesis, which was consistent with very limited influence of weathering and metamorphism that could affect such sediments (Liang C. et al., 2018). This viewpoint is supported by the fact that interbedded carbonates and mudstones have consistently yielded similar redox interpretations across all instances of rock samples (Raiswell et al., 2018). Generally, the unusually high dolomite content in fine-grained sediments should indicate rather atypical lacustrine chemistry due to volcanism, hydrothermal fluids, or transgressions that may affected variability in calcium carbonate saturation leading to dolomite rather than calcite precipitation (Zhang et al., 2018; Liu et al., 2021).

5. Discussion

5.1. High primary productivity in middle Eocene warmhouse

Compared to the unmineralized fraction in deep sediments of modern large lakes and marine sediments (Galazzo et al., 2013; Liu et al., 2019, 2021), our high TOC values (average 4%) may indicate that the primary productivity of the lake over the entire interval (Es_4^1 to Es_3^3) was indeed higher than that during other MECO intervals (1−3% TOC; Galazzo et al., 2013). Algae-rich sediments worldwide are well-known to be a product of high primary productivity (Meyers, 1997). In Jiyang paleolakes,

algae-rich sedimentary layers, formed by alternating blooms of coccolithophytes and dinoflagellates, were a major feature of the Paleogene oil source rocks in the Bohai Bay Basin for more than 1 Ma (Xie et al., 2016; Song et al., 2020; Shi et al., 2021). These algal blooms are well recognized in the middle Eocene warming period of the Cenozoic (Bijl et al., 2010; Zachos et al., 2008; Pearson, 2010), which occurred 41.4−39.2 Ma ago (Shi et al., 2019). During this time, a warm climate and associated high productivity were favorable for oxygen consumption beneath the photic zone. The water column became anoxic, thereby leading to enhanced preservation and burial of organic matter. High productivity can be supported by systematically elevated concentrations of both TOC and barium (Zeng et al., 2018). TOC values above 6% are recorded here over 11 intervals across the depth range 3343.47 to 3102.67 m, with two intervals having TOC values as high as 8.4% and 10.4% at 3176.51 m and 3192.90 m, respectively (Fig.2). The average Ba concentrations in Es_4^1 and Es_3^3 are 470 and 560 ppm, respectively. Over the entire section in the Jiyang Depression, Ba values in samples positively correlate with the corresponding TOC values (Supplementary Table 2). For comparison, in a similar high paleoproductivity Lake Malawi (East Africa), the TOC concentrations are ~ 6 % in the sediments from the anoxic deep parts of the lake (Li et al., 2018).

Meanwhile, high primary productivity can also be confirmed by organic carbon isotope values. Most samples show $\delta^{13}C_{org}$ values between -29‰ and -25‰, indicating a source of lacustrine organic matter from exogenous terrestrial plants, authigenic phytoplankton photosynthesis, as well as possible allochthones (Meyers, 1997). Terrestrial C4 plants were very rare in the Jiyang Depression during the middle Eocene

as they are usually found in dry environments and have the $\delta^{13}C_{org}$ values higher than -20‰. However, there might have been some C3 plants in the lake, because small fragments of higher plants (including leaves) can be windblown and floating debris could sink, although some of the compounds of terrestrial origin may have been subsequently degraded by diagenesis. In the detailed core observations of the FY1 well, over a total length of 403.6 m, no fragments of higher plants were observed. Generally, there is no direct relationship between the concentration of biomarkers and the source of organic matter because many biomarkers can be detected at very low concentrations. There was probably some retene, oleanene, or β-carotene (Xu et al., 2020); however, the contribution of higher plants to the preserved organic matter is expected to be small. For another, the relative content of the biomarkers may also change further with diagenesis. For example, Xu et al. (2020) also proposed an existing algae source of retene, oleanene, or β-carotene during organic-rich shale formation. To sum up, the contribution of organic matter of terrestrial origin from higher plants depends on the lake size and sedimentation process. In a very large paralic lake continental runoff input can be significant only due to strong storms, floods or other events from land. As there were no land events in the Jiyang Depression with a total area of 26,000 km^2, the detected compounds of higher plants do not mean that the terrestrial organic input is significant in this offshore lake.

Combined with the sedimentary characteristics of modern lakes, we propose that in the center of the paralic Jiyang lake like FY-1 Well, the organic matter may mainly come from lacustrine authigenesis, the input of terrigenous organic matter, such as plants, may only have occurred in brief periods. Of the studied 270 samples, only a few

(25 in Es_3^3 and 27 in Es_4^1) showed $\delta^{13}C_{org}$ values above -25‰, with an average TOC of 5% (Fig.2), indicating that during this period organic matter may have been occasionally derived from very limited amount of terrestrial plants. Thus, most of the organic matter enrichment in the source rocks of the Shahejie Formation likely resulted from native algal and bacterial production coupled with favorable preservation conditions. Due to a globally significant increase of greenhouse gases in the MECO atmosphere (Bijl et al., 2010), photosynthetic carbon fixation could lead to carbon isotope ratios as low as −29‰ (Hodell and Schelske, 1998). Therefore, we propose that the negative excursions of $\delta^{13}C_{org}$ corresponded to high primary productivity during warm and humid climate caused by periods of elevated atmospheric pCO_2. Under these elevated pCO_2, CO_2 was predominantly transported into lacustrine systems via photosynthesis, and was reduced by biological processes into organic matter with enrichment in the lighter isotope (^{12}C), thereby yielding negative excursions of $\delta^{13}C$ values.

5.2. Ferruginous/euxinic water conditions

Lallier-Verges et al. (1993) quantified the degree of bacterial sulfate reduction (BSR) using the sulfate reduction index (SRI), which is defined as the ratio of primary organic carbon to residual organic carbon. Primary organic carbon encompasses both the organic carbon depleted via sulfate reduction, and the residual total organic carbon (TOC (wt.%) at present). Organic carbon loss (C_{loss}) by degradation coupled with sulfate reduction may be assessed from the stoichiometry of the sulfate reduction equation proposed by Berner and Raiswell (1984):

$$SRI = (TOC + C_{loss})/TOC \quad (1)$$

$$\text{where } C_{loss} = TS/1.33 \quad (2)$$

Substituting (2) into (1) yields:

$$SRI = (TOC + TS/1.33)/TOC = 1 + 0.75 \times TS/TOC \quad (3)$$

The SRI is regarded as the lowest degradation consumption index for total organic carbon. The higher the BSR activity, the higher the SRI value, and the greater the organic matter consumption. For SRI < 1.375, the BSR intensity can be limited by total sulfate and the amount of undegraded TOC may increase substantially. For SRI > 1.375, the BSR intensity increases, and the overall TOC value is relatively low (Liu et al., 2021). The relationship between the sulfate reduction strength and the organic carbon content (SRI/TOC) in the study interval shows that most of the SRI values in the ferruginous water column are less than 1.375 (Fig. 4 (D)), indicating a weak sulfate reduction, which may have been conductive to organic matter preservation and burial. In contrast, euxinic waters with strong BSR may result both in organic preservation and consumption. It can be seen in Fig. 3 and 4 (D) that in the euxinic zone, most samples with TOC < 2 % have SRI values > 1.375.

Several mechanisms may have created ferruginous conditions at the bottom of the Jiyang lake. A combination of volcanism, hydrothermal fluids, and transgression may have brought reactive iron and maintained anoxic conditions, while the primary productivity was high. For example, volcanism could have increased nutrient influxes (Liu et al., 2019, 2024), and productivity, and stimulated oxygen consumption below the photic zone. Meanwhile, the isotopically “light” sulfur ($\delta^{34}S_{py}$ of 0 ‰) from a volcanic source was preferentially utilized by BSR, resulting in low $\delta^{34}S_{py}$ values.

However, intermittent sulfidization events in a ferruginous Jiyang Lake may not have led to elevated Fe_{py}/Fe_{HR} ratios compared to typical marine values of 0.7, because such an increase may be obscured by the high carbonate (Fe_{carb}) content largely dominating over Fe_{py} (Fig. 2, Unit 2, 3, 5). For all the samples, there are only two Fe_{py}/Fe_{HR} values above 0.7, with the corresponding $\delta^{34}S_{py}$ values of 24−25‰) (Fig. 4 A, C). The two $\delta^{34}S_{py}$ values, higher than those in the lower adjacent interval (~13 ‰), indicate that the basin became relatively closed and euxinic after a period of volcanism or hydrothermal activity. The positive $\delta^{34}S_{py}$ values (> 20‰) are higher than the sulfate ^{34}S from seawater during middle Eocene, indicating the depletion of the light sulfur isotopes in sulfate under strong BSR. Meanwhile, the TOC values for these two samples are 3.4 and 2.8% at 3332.39 and 3226.24 m, respectively (Fig. 2), which are less than the average value (4.0%) of the study interval, indicating that BSR consumed the primary organic matter and converted sulfate to H_2S, and promoted pyrite formation. A rough positive covariation between the Fe_{py}/Fe_{HR} ratios and TOC also supports the BSR occurrence (Fig. 4 A, B). However, the high TOC/TS ratios (> 2.0) and low sulfate reduction index (SRI) (< 1.375) suggest that it was sulfate availability, rather than organic matter supply, that constrained BSR in deep waters (Fig. 4 (D)).

For Jiyang Lake, there may have been occasional euxinic conditions as the TOC/TS values are less than 2 (in 36 samples from 270). Euxinia in the photic zone (from biomarker data) and deeper water (based on framboid size distributions) has been identified in Silurian, Devonian, Permian and Eocene oceans (Racka et al., 2010; Marynowski et al., 2012; Liu et al., 2019; Xu et al., 2020; Percival et al., 2022). Euxinia is prevalent in anoxic marine environments where sulfate is abundant. Modern

meromictic lakes develop euxinia when sulfate concentrations exceed 100 μM, while below that threshold their monimolimnia (the deep stagnant layers) tend to be ferruginous. Xu et al. (2020) demonstrated that there were different euxinic water conditions during the deposition of the Shahejie Formation, evidenced by variations in the aryl isoprenoid ratio, relative amount of isorenieratane, long-chain n-alkane carbon isotopic composition and other molecular indicators, which indicated different intensity of bacterial sulfate reaction (BSR). In Jiyang Lake, potential sources for extra sulfate could have been episodic (for 5−10 ka) marine transgressions (Unit 2 and Unit 5), volcanism (Unit 1, 2, 3 of Es_4^1, and Unit 5 of Es_3^3) or hydrothermal fluids (Unit 4 of Es_3^3) (Fig. 2). Outside these episodes, sulfate would become depleted by BSR, Fe_{py}/Fe_{HR} values were mostly < 0.6 and Fe_{HR}/Fe_T values > 0.38 (Fig.4 A), which also suggests that the deep-water column throughout the middle Eocene was predominantly ferruginous. Meanwhile, there might also be very occasional oxic episodes identified by the presence of bioturbation in anoxic brackish water (Song et al., 2020). Although Fe shuttling could potentially create local enrichments of Fe_{carb} (Fig.4 (B)) or Fe_{ox}, resulting in high Fe_{HR}/Fe_T and low Fe_{py}/Fe_{HR} ratios, the deep lake was probably anoxic and ferruginous during most of the depositional period. The reduced Fe transported from the anoxic water column could have led to Fe_{carb} enrichments in bioturbated sediments. As anoxic ferruginous conditions expanded and contracted over time, reactive iron enrichment could form in even deeper settings.

In summary, the Fe_{HR} values between 1.2% and 6.6% generally show the same evolution trend as the total of Fe_{py} and Fe_{carb}, while Fe_{ox} and Fe_{mag} have little correlation with the Fe_{HR} content trend. Thus, organic matter enrichment was primarily created by

both enhanced preservation under ferruginous water conditions and high paleo-productivity with limited dilution of the shale by terrigenous clastic materials (Xie et al., 2016; Song et al., 2020).

5.3. Impacts of geological events on organic carbon burial

Our core analyses demonstrate that volcanism, hydrothermal activity, and marine transgressions affected the study area. Only few investigations of carbon and pyrite sulfur isotopic variations focused on lacustrine sedimentary intervals during the MECO. Our study uses different covariations between $\delta^{34}S_{py}$ and $\delta^{13}C_{org}$ values (Fig. 2B, D) to establish a relationship between geological events, biological productivity, and water redox conditions. It has been shown that a negative excursion of 2 to 6‰ in $\delta^{13}C_{org}$ of both carbonate and organic carbon is linked to global volcanism (Lee et al., 2018; Liu et al., 2019; Longman et al., 2019; Shen J. et al., 2019b; Li Y. et al., 2021). Indeed, in the study intervals, volcanism effects are evident in nine prominent negative excursions in $\delta^{13}C_{org}$ (Fig. 2B), which are correlated with tuff interlayers (Fig. 5). The pyroclastic interlayers in the shales are predominantly vitreous and crystalline debris of andesite (Fig. 5 (C, D)), in which microfractures were developed and ostracod fragments were deposited. Such negative excursions in $\delta^{13}C_{org}$ values are typically associated with increases in primary productivity, which can be brought about by the increased delivery of nutrients following the volcanic events.

The same layers with highly negative $\delta^{13}C_{org}$ are also associated with negative shifts in $\delta^{34}S_{py}$ (as low as 8.9‰; Fig. 2D). The water column in the deep lake was usually closed when there were no geological events. In this case, the SO_4^{2-} reservoir is limited and could not be replenished. With the continuing exhaustion of the sulfate

reservoir (enriched in ^{34}S) by sulfur reduction through dissimilation, $^{34}S_{py}$ gradually increased and approached that of the initial sulfate. In contrast to open marine sediments, $^{34}S_{py}$ values in an almost infinite sea water sulfate reservoir, are usually below 0‰ (Li et al., 2021). Volcanic and hydrothermal activity generate sulfur with $\delta^{34}S$ of 0 to 5‰ (Huston, 1999), which is substantially below the values of water surface-sourced sulfate (~ 20‰ during study period). If sub-lacustrine eruptions of a volcano or associated geothermal fluids carried $H_2{}^{32}S$-enriched sulfide sulfur into a closed lake, its reaction with highly reactive iron could form isotopically equivalent $Fe^{32}S_2$-enriched pyrite within a quite short period of time (i.e. several years). This process caused the decrease in $\delta^{34}S_{py}$ values along with the sulfate of the light sulfur isotope was consumed by BSR. As volcanic $H_2{}^{32}S$ was quickly consumed by iron and the BSR began to reduce sulfate in a closed system, the resulting pyrite had lighter $\delta^{34}S$ values. Higher $\delta^{34}S_{py}$ values then formed again at low sulfate concentrations at the end of sulfate reduction. If volcanic activities or deep fluids carried large amounts of oxidized volatiles, such as SO_2, BSR would have been enhanced and more ^{32}S consumed. As a result, $^{34}S_{py}$ first decreased and then increased with an increased amount of sulfate consumption. Indeed, this trend could be identified especially in Units 1 and 3 of Es_4^1 (Fig. 2D). Because the bottom waters of the paleolake seemed to have remained ferruginous, the iron input (as Fe (II); Isley and Abbott, 1999; Kump and Seyfried, 2005) during these volcanic or hydrothermal activities must have exceeded the inputs of sulfur into the lake.

The presence of marine ostracods (Fig 5 (A)), elevated $\delta^{34}S_{py}$ values (~20 ‰) and high carbonate content (Fe_{carb} to ~5%) collectively indicate marine transgressions,

which is consistent with the interpretation of the strata using the method of astronomical cycles (Ma et al., 2023). During middle Eocene warming, marine transgressions increased the lake water depth and supplied ^{34}S-enriched sulfate, causing the $\delta^{34}S_{py}$ value of pyrite to approach that of seawater. The $\delta^{34}S_{py}$ values vary between 9 and 36 ‰, being both lower and higher than those of the marine sulfates identified during the MECO (20.9 ± 0.5‰; Longinelli, 1989; Kampschulte et al., 2001). Marine transgressions may have occurred roughly every 1,000 years over a period of 5,000 years (Fig. 2, Units 2 and 5). As BSR generates isotopically light sulfide, the heavier $\delta^{34}S_{py}$ values can be attributed to the consumption of sulfate sulfur after staged transgression when the lake system closed again. Mineral analyses show that the total content of Fe_{mag} and Fe_{ox} is low, with a maximum of 0.37%, so the contents of ferrous carbonate and pyrite compete with each other. This is consistent with most sediments in modern paralic environment (Liu et al., 2023; Zhang et al., 2024). Only the difference between the samples of the two study areas is the contents of ferrous carbonate, indicating the different water conditions during their sediment deposition. In Shahejie Formation, the carbonate content in the study interval was generally high, with average calcite and dolomite contents of 37% and 10%, respectively. For example, the content of Fe_{carb} is higher than that of Fe_{py} from 3225 to 3200 m in Unit 5 (Fig.2), indicating that the sulfur isotope fractionation of pyrite in the paralic lakes during the sulfate reduction process was constrained by changes in the global sea level. The sea level increased in the warm and humid climate, and transgression brought large amounts of Ca^{2+} to form carbonates. Meanwhile, high paleo-productivity also promoted the deposition of organic-rich layers. Therefore, the precipitation of calcium

carbonate and organic matter layers is the result of increased pH due to strong photosynthesis by algae in the warm climate during marine transgressions in the Jiyang calcareous lake. After that, the organic matter was degraded in a limited manner under ferruginous conditions and was well preserved.

The delicate equilibrium between ferruginous and euxinic chemical conditions could be influenced by the comparable rates of Fe_{HR} and sulfate input fluxes. On a global scale, continental sources stand out as the primary contributors to the potential Fe_{HR} flux. At the regional scale, geological events, such as volcanic activity or ocean transgression, could also have liberated some reactive iron and sulfate into the lake, providing a conceivable mechanism for the transportation of ferrous iron and resulting in a disproportionate increase in the Fe_{HR} flux relative to that of sulfate. The interplay of all these processes have generated dominantly ferruginous environments during the middle Eocene in the Jiyang Depression.

On the basis of the aforementioned research, we propose that there was an extensive burial of lacustrine organic carbon in Eastern China during the warm and humid climate of the middle Eocene, which thereby created a positive feedback loop in the Earth's climate system. Frequent volcanic activity during the early stages of Es_4^1 might have brought aerosols to increase the albedo in the short-term cold climate (Fig.6B, maybe to 10 years). Most importantly, it released abundant CO_2 into in the atmosphere and brought reactive iron and nutrients to create optimal environments for the growth and expansion of algae and plankton in the later stages (Fig.6A, to 1 million years) of the middle Eocene. As temperatures increased, the biological productivity in Jiyang Lake increased, leading to enhanced production of total organic carbon in

ferruginous water conditions. This positive feedback mechanism may have contributed to the sustained warmth of the middle Eocene climate. Based on this analysis, we highlight a combined effect on sedimentation of external events such as input of volcanic ash, intermittent hydrothermal fluids and marine transgressions during middle Eocene continental warming of western Pacific. These events could not only supply nutrients and catalytic elements to promote biological productivity and cause oxygen consumption, but they also enhanced the reactive iron input to form the dynamic anoxic ferruginous conditions that were conducive for the preservation of organic carbon.

6. Conclusions

The widespread terrestrial sedimentary and geochemical records of the middle Eocene in the Eastern China have been established using novel TOC, TS, iron speciation, $\delta^{13}C_{org}$ and $\delta^{34}S_{py}$ data. These data, including the highly-reactive iron to total iron ratios ($Fe_{HR}/Fe_T > 0.38$), along with a wide range of total organic carbon content (TOC, from 1 to 10 %) exceeding that of total sulfur (TOC/TS > 2), and low sulfate reduction indexes (SRI < 1.375), collectively suggest widespread anoxic and ferruginous conditions that would have been favorable for burial of lacustrine organic carbon during the middle Eocene in the paralic lacustrine environments of the Jiyang Depression. The temporal stability of lacustrine ferruginous water conditions may have been due to the warm and humid climate during the middle Eocene, with high biological productivity and large oxygen consumption in the water column, leading to efficient burial of organic carbon in deep sediments.

Both $\delta^{13}C_{org}$ and $\delta^{34}S_{py}$ values reveal transient geological events such as volcanism,

hydrothermal fluids, and transgressions. Negative $\delta^{13}C_{org}$ and $\delta^{34}S_{py}$ excursions along the sedimentary column point to transient volcanic events, whereas positive $\delta^{13}C_{org}$ along with negative $\delta^{34}S_{py}$ excursions indicate injection of associated hydrothermal fluids; in contrast, elevated $\delta^{34}S_{py}$ (to ~20‰) point to frequent marine transgressions. Despite potential inputs of sulfur into the paleolake as a result of these geological events, bacterial sulfate reduction efficiently consumed the sulfate pool, thereby creating ferruginous water conditions favorable for the efficient preservation of organic carbon.

Acknowledgments

We thank Yunqing Hao for assistance with microscopic slice analyses and for discussions, Prof. Chao Li and Prof. Yan'an Shen for help with the geochemical analyses, Prof. Bing Shen and Dr. Huiyuan Xu for discussions. This work was supported by the National Natural Science Foundation of China (Grants 42172151, 41811530094, and 41625009), the China Postdoctoral Science Foundation (Grant 2021M690204), and the National Key Research and Development Program (Grant 2023YFF0806200). We thank the two reviewers and the editorial support for the constructive comments, which have greatly improved the quality of this paper.

Research Data

All of the processed data discussed has been uploaded in the supplementary tables.

References

Berner, R. A., Raiswell, R.,1984. C/S method for distinguishing freshwater from marine sedimentary

rocks. Geology 12 (6), 365–368. DOI: 10.1130/0091-7613(1984)12<365:CMFDFF>2.0.CO;2
Bhattarai, S., Ross, K.A., Schmid, M., Anselmetti, F.S., Bürgmann, H., 2012. Local Conditions Structure Unique Archaeal Communities in the Anoxic Sediments of Meromictic Lake Kivu. Microb. Ecol. 64 (2), 291–310. DOI: 10.1007/s00248-012-0034-x
Bijl, P.K., Houben, A.J.P., Schouten, S., Bohaty, S.M., Sluijs, A., Reichart, G.J., Sinninghe D.J., Brinkhuis, H., 2010. Transient middle Eocene atmospheric CO_2 and temperature variations. Science 330 (6005), 819–821. DOI: 10.1126/science.1193654
Clarkson, M.O., Poulton, S.W., Guilbaud, R., Wood, R., 2014. Assessing the utility of Fe/Al and Fe-speciation to record water column redox conditions in carbonate-rich sediments. Chem. Geol. 382, 111–122. DOI: 10.1016/j.chemgeo.2014.05.031
Clarkson, M.O., Wood, R.A., Poulton, S.W., Richoz, S., Newton, R.J., Kasemann, Bowyer, F., Krystyn, L., 2016. Dynamic anoxic ferruginous conditions during the end-Permian mass extinction and recovery. Nat. Commun. 7, 12236. DOI: 10.1038/ncomms12236
Duggen, S., Olgun, N., Croot, P., Hoffmann, L., Dietze, H., Teschner, C., 2010. The role of airborne volcanic ash for the surface ocean biogeochemical iron-cycle: a review. Biogeosciences 7, 827–844. DOI: 10.5194/bgd-6-6441-2009
Galazzo, B.F, Giusberti, L, Luciani, V, Thomas, E., 2013. Paleoenvironmental changes during the Middle Eocene Climatic Optimum (MECO) and its aftermath: The benthic foraminiferal record from the Alano section (NE Italy). Palaeogeogr. Palaeoclimatol. Palaeoecol. 378, 22–35. DOI: 10.1016/j.palaeo.2013.03.018
Guilbaud, R., Poulton, S.W., Butterfield, N.J., Zhu, M., Shields-Zhou, G.A., 2015. A global transition to ferruginous conditions in the early Neoproterozoic oceans. Nat. Geosci. 8(6), 1–5. DOI: 10.1038/ngeo2434
He, R., Lu, W., Junium, C.K., Straeten, C.A.V., Lu, Z., 2020. Paleo-redox context of the Mid-Devonian Appalachian Basin and its relevance to biocrises. Geochim. Cosmochim. Acta 287, 328–340. DOI: 10.1016/j.gca.2019.12.019
Hodell, D.A., Schelske, C.L., 1998. Production, sedimentation, and isotopic composition of organic matter in Lake Ontario. Limnol. Oceanogr. 43, 200–214. https://doi.org/10.4319/lo.1998.43.2.0200
Huston., David L., 1997. Stable Isotopes and Their Significance for Understanding the Genesis of Volcanic-Hosted Massive Sulfide Deposits: A Review. Volcanic Associated Massive Sulfide Deposits: Processes and Examples in Modern and Ancient Settings, C. Tucker Barrie, Mark D. Hannington. https://doi.org/10.5382/Rev.08.07
Isley, A.E., Abbott, D.H., 1999. Plume-related mafic volcanism and the deposition of banded iron formation. J. Geophys. Res.: Solid Earth. 104 (B7), 15461–15477. https://doi.org/10.1029/1999JB900066
Jovane, L., Florindo, F., Coccioni, R., Dinarès-Turell, J., Marsili A., Monechi, S., Roberts, A., Sprovieri, M., 2007. The middle Eocene climatic optimum event in the Contessa Highway section, Umbrian Apennines, Italy. GSA Bull. 119 (3-4), 413–427. DOI: 10.1130/B25917.1
Kampschulte, A., Bruckschen, P., Strauss, H., 2001. The Sulphur isotopic composition of trace sulphates in Carboniferous brachiopods: implications for coeval seawater, correlation with other geochemical cycles and isotope stratigraphy. Chem. Geol., 175 (1), 149-173. DOI: 10.1016/S0009-2541(00)00367-3
Kim, T.Y., North, R.L., Guildford, S.J., Dillon, P., Smith, R.E.H., 2015. Phytoplankton productivity and size composition in Lake Simcoe: The nearshore shunt and the importance of autumnal production. J. Great Lakes Res. 41 (4), 1075–1086. https://doi.org/10.1016/j.jglr.2015.09.011

577 Kump, L. R., Seyfried, W. E., 2005. Hydrothermal Fe fluxes during the Precambrian: effect of low
578 oceanic sulfate concentrations and low hydrostatic pressure on the composition of black smokers.
579 Earth Planet. Sci. Lett. 235, 654–662. DOI: 10.1016/j.epsl.2005.04.040
580 Lallier-Verges, E., Bertrand, P., Desprairies, A., 1993. Organic matter composition and sulfate
581 reduction intensity in Oman Margin sediments. Mar. Geol., 112, 57–69. DOI: 10.1016/0025-
582 3227(93)90161-N
583 Langmann, B., Zaksek, K., Hort, M., Duggen S., 2010. Volcanic ash as fertiliser for the surface ocean.
584 Atmos. Chem. Phys. 10, 3891–3899. DOI: 10.5194/acp-10-3891-2010
585 LaRowe, D.E., Arndt, S., Bradley, J.A., Estes, E.R., Hoarfrost, A., Lang, S.Q., Lloyd, K.G.,
586 Mahmoudi, N., Orsi, W.D., Shah, W.S.R., Steen. A.D., Zhao. R., 2020. The fate of organic
587 carbon in marine sediments - New insights from recent data and analysis. Earth Sci. Rev. 204,
588 103146. DOI: 10.1016/j.earscirev.2020.103146
589 Layton-Matthews, D., Leybourne, M.I., Peter, J.M., Scott, S.D., Cousens, B., Eglington, B.M., 2013.
590 Multiple sources of selenium in ancient seafloor hydrothermal systems: Compositional and Se,
591 S, and Pb isotopic evidence from volcanic-hosted and volcanic-sediment-hosted massive sulfide
592 deposits of the Finlayson Lake District, Yukon, Canada. Geochim. Cosmochim. Acta 117, 313–
593 331. DOI: 10.1016/j.gca.2013.05.002
594 Lee, C-T.A., Jiang, H., Ronay, E., Minisini, D., Stiles, J., Neal, M., 2018. Volcanic ash as a driver of
595 enhanced organic carbon burial in the Cretaceous. Sci. Rep. 8, 4197. DOI: 10.1038/s41598-018-
596 22576-3
597 Li, J., Brown, E.T., Crowe, S.A., Katsev, S., 2018. Sediment geochemistry and contributions to
598 carbon and nutrient cycling in a deep meromictic tropical lake: Lake Malawi (East Africa). J.
599 Great Lakes Res. 44: 1221–1234. https://doi.org/10.1016/j.jglr.2017.12.001
600 Li, Y., Zhang, T., Shen, B., Li, Z., Shao, D., Lash, G.G., 2021. Carbon and sulfur isotope variations
601 through the Upper Ordovician and Lower Silurian of South China linked to volcanism.
602 Palaeogeogr. Palaeoclimatol. Palaeoecol. 567, 110285. DOI: 10.1016/j.palaeo.2021.110285
603 Liang, C., Jiang, Z.X., Cao, Y.C., Wu, J., Wang, Y.S., Hao, F., 2018, Sedimentary characteristics and
604 origin of lacustrine organic-rich shales in the salinized Eocene Dongying Depression. GSA
605 Bulletin 130 (1-2):154–174. DOI: 10.1130/B31584.1
606 Liang, J., Wang, H., Bai, Y., Ji, X., Duo, X., 2016. Cenozoic tectonic evolution of the Bohai Bay
607 Basin and its coupling relationship with Pacific Plate subduction. J Asian Earth Sci 127, 257–
608 266. http://dx.doi.org/10.1016/j.jseaes.2016.06.012
609 Liang, X., Jin Z., Philippov, V.P., Obryadchikov, O.S., Zhong, D., Liu, Q., Uspensky, B., Morozov,
610 V., 2020. Sedimentary features of Domanik shelf carbonate measures during regression in the
611 southeastern Volga-Ural basin. Mar. Petrol. Geol. 2020, 119, 104438. DOI:
612 10.1016/j.marpetgeo.2020.104438
613 Liu, Q, Zhu, D, Meng, Q, Liu, J, Wu, X, Zhou, B, Fu, Q, Jin, Z. 2019. The scientific connotation of
614 oil and gas formations under deep fluids and organic-inorganic interaction. Sci. China Earth Sci.
615 62: 507–528. DOI: 10.1007/s11430-018-9281-2
616 Liu, Q., Li, P., Jin, Z., Liang, X., Zhu, D., Wu, X., Meng, Q., Liu, J., Fu, Q., Zhao, J., 2021.
617 Preservation of organic matter in shale linked to bacterial sulfate reduction (BSR) and volcanic
618 activity under marine and lacustrine depositional environments. Mar. Petro. Geol. 127,
619 2021,104950. DOI: 10.1016/j.marpetgeo.2021.104950
620 Liu, Q., Li, P., Jiang, L., Jin, Z., Liang, X., Zhu, D., Pang, Q., Zhang, R., Liu, J., 2024. Distinctive
621 volcanic ash–rich lacustrine shale deposition related to chemical weathering intensity during the
622 Late Triassic: Evidence from lithium contents and isotopes. Sci. Adv. 10 (11), 1–9. DOI:

10.1126/sciadv.adi6594
Liu, X., Hu, Y., Dong, J., Li, A., Zhuang, G., Wang, H., 2023. Iron-bearing minerals indicate sea-level rise of the East China Sea inner shelf since the last deglaciation. Sci. Bull. 68(4), 364–366. https://doi.org/10.1016/j.scib.2023.02.002
Longinelli, A., 1989. Oxygen-18 and sulphur-34 in dissolved oceanic sulphate and phosphate. In: Fritz, P., Fontes, J.C., (eds), Handbook of environmental isotope geochemistry, 3. Elsevier, Amsterdam, 221–255. Illustration, Table; ref: 7p, ISSN 0167-949X http://pascal-francis.inist.fr/vibad/index.php?action=getRecordDetail&idt=7227509
Longman, J., Palmer, M.R., Gernon, T.M., Manners, H.R., 2019. The role of tephra in enhancing organic carbon preservation in marine sediments. Earth Sci. Rev. 192, 480–490. DOI: 10.1016/j.earscirev.2019.03.018
Lourens, L.J., Sluijs, A., Kroon, D., Zachos, J.C., Thomas, E., Röhl, U., Bowles, J., Raffi, I., 2005. Astronomical pacing of late Palaeocene to early Eocene global warming events. Nature 435, 1083–1087. DOI: 10.1038/nature03814
Lyons, T.W., Severmann, S., 2006. A critical look at iron paleoredox proxies: New insights from modern euxinic marine basins. Geochim. Cosmochim. Acta 70, 5698–5722. DOI: 10.1016/j.gca.2006.08.021
Ma, Y, Fan, M., Li, M., Ogg, J., Zhang, C., Feng, J., Zhou, C., Liu, X., Lu, Y., Liu, H., Eldrett, J.S., Ma, C., 2023. East Asian lake hydrology modulated by global sea-level variations in the Eocene warmhouse. Earth Planet. Sci. Lett. 602, 117925. DOI: 10.1016/j.epsl.2022.117925
Magnall, J.M., Gleeson, S.A., Blamey, N.J.F., Paradis, S., Luo, Y., 2016. The thermal and chemical evolution of hydrothermal vent fluids in shale hosted massive sulphide (SHMS) systems from the MacMillan Pass district (Yukon, Canada). Geochim. Cosmochim. Acta 193, 251–273. DOI: 10.1016/j.gca.2016.07.020
Malumián, N., Ramos, V.A.,1984. Magmatic intervals, transgression-regression cycles and oceanic events in the Cretaceous and Tertiary of southern South America. Earth Planet. Sci. Lett., 67 (2), 228–237. DOI: 10.1016/0012-821X(84)90118-3
Marynowski, L., Zatoń, M., Rakociński, M., Filipiak, P., Kurkiewicz, S., Pearce, T.J., 2012. Deciphering the upper Famennian Hangenberg Black Shale depositional environments based on multi-proxy record. Palaeogeogr. Palaeoclimatol. Palaeoecol. 346-347, 66–86. DOI: 10.1016/j.palaeo.2012.05.020
Meyers, P.A., 1997. Organic geochemical proxies of paleoceanographic, paleolimnologic, and paleoclimatic processes. Org. Geochem. 27(5–6), 213–250. DOI: 10.1016/S0146-6380(97)00049-1
Paytan, A., M. Kastner, D., Campbell, M.H. Thiemens, 1998. Sulfur isotope composition of Cenozoic seawater sulfate. Science 282, 1459-1462.
Pearson P.N., 2010. Increased Atmospheric CO_2 During the Middle Eocene. Science Science 330 (6005), 763–4. DOI: 10.1126/science.1197894
Percival, L.M.E., Marynowski, L., Baudin, F., Goderis S., Vleeschouwer D. De, Rakociński M., Narkiewicz K., Corradini C., Silva A. C. Da, Claeys P., 2022. Combined Nitrogen-Isotope and Cyclostratigraphy Evidence for Temporal and Spatial Variability in Frasnian–Famennian Environmental Change. Geochem. Geophys. Geosys. 23(5), e2021GC010308 DOI: https://doi.org/10.1029/2021GC010308
Planavsky, N.J., McGoldrick, P., Scott, C.T., Li, C., Reinhard, C.T., Kelly, A.E., Chu, X., Bekker, A., Love, G.D., Lyons, T.W., 2011. Widespread iron-rich conditions in the mid-Proterozoic ocean. Nature 477, 448–451. DOI: 10.1038/nature10327

669 Ploeg, R.V.D., Cramwinckel, M. J., Kocken, I. J., Leutert, T. J., Bohaty, S. M., Fokkema, C. D., Hull,
670 P. M., Meckler, A. N., Middelburg, J. J., Müller, I. A., Penman, D. E., Peterse, F., Reichart, G.-
671 J., Sexton, P. F., Vahlenkamp M., Vleeschouwer, D. D., Wilson, P. A., Ziegler, M., Sluijs, A.,
672 2023. North Atlantic surface ocean warming and salinization in response to middle Eocene
673 greenhouse warming. Sci. Adv. 9, eabq0110. DOI: 10.1126/sciadv.abq0110
674 Poulton, S.W., Canfield, D.E., 2005. Development of a sequential extraction procedure for iron:
675 Implications for iron partitioning in continentally derived particulates. Chem. Geol. 214, 209–
676 221. DOI: 10.1016/j.chemgeo.2004.09.003
677 Poulton, S.W., Canfield, D.E., 2011. Ferruginous conditions: A dominant feature of the ocean through
678 Earth's history. Elements 7, 107–112. DOI: 10.2113/gselements.7.2.107
679 Poulton, S.W., 2021. The Iron Speciation Paleoredox Proxy: Elements in Geochemical Tracers in
680 Earth System Science: New York, Cambridge University Press, 24 p.
681 https://doi.org/10.1017/9781108847148.
682 Racka M., Marynowski L., Filipiak P., Sobstel M., Pisarzowska A., Bond D. P.G., 2010. Anoxic
683 Annulata Events in the Late Famennian of the Holy Cross Mountains (Southern Poland):
684 Geochemical and palaeontological record. Palaeogeogr. Palaeoclimatol. Palaeoecol. 297(3-4),
685 549–575. DOI: 10.1016/j.palaeo.2010.08.028
686 Raiswell, R., Hardisty, D.S., Lyons, T.W., Canfield, D.E., Owens, J.D., Planavsky, N.J., Poulton,
687 S.W., Reinhard, C.T.,2018. The iron paleoredox proxies: A guide to the pitfalls, problems and
688 proper practice. Am. J. Sci. 318 (5), 491–526. DOI: 10.2475/05.2018.03
689 Ross, K. A., Smets, B., Batist, M.D., Hilbe, M., Schmid, M., Anselmetti, F.S., 2014. Lake-level rise
690 in the late Pleistocene and active subaquatic volcanism since the Holocene in Lake Kivu, East
691 African Rift. Geomorphology, 221, 274–285. DOI: 10.1016/j.geomorph.2014.05.010
692 Ruebsam, W., Pieńkowski, G., Schwark, L., 2020. Toarcian climate and carbon cycle perturbations
693 – its impact on sea-level changes, enhanced mobilization and oxidation of fossil organic matter.
694 Earth Planet. Sci. Lett. 546, 116417. DOI: 10.1016/j.epsl.2020.116417
695 Shen, J., Yu, J.X., Chen, J.B., Algeo, T.X., Xu, G.Z., Feng, Q.L., Shi, X., Planavsky, N.J., Shu, W.C.,
696 Xie, S.C., 2019. Mercury evidence of intense volcanic effects on land during the Permian-
697 Triassic transition. Geology. 47, 1117–1121.
698 Shen, W., Shao, L., Zhou, Q., Liu, J., Eriksson, K.A., Kang, S. and Steel, R.J., 2024. The role of
699 fluvial and tidal currents on coal accumulation in a mixed-energy deltaic setting: Pinghu
700 Formation, Xihu Depression, East China Sea Shelf Basin. Sedimentology, 71: 173-206.
701 https://doi.org/10.1111/sed.13133
702 Shen, Y., Knoll, A.H., Walter, M.R., 2003. Evidence for low sulphate and anoxia in a mid-Proterozoic
703 marine basin. Nature 423, 632–635. DOI: 10.1038/nature01651
704 Shi, J., Jin, Z., Liu, Q., Zhang, R., Huang, Z., 2019. Cyclostratigraphy and astronomical tuning of the
705 middle Eocene terrestrial successions in the Bohai Bay Basin, Eastern China. Global Planet.
706 Change 174, 115–126. DOI: 10.1016/j.gloplacha.2019.01.001
707 Song, M., Liu, H., Wang, Y., Liu, Y., 2020. Enrichment rules and exploration practices of Paleogene
708 shale oil in Jiyang Depression, Bohai Bay Basin, China. Petrol. Explor. Develop. 47 (2), 242–
709 253. DOI: 10.1016/S1876-3804(20)60043-X
710 Swanner, E.D., Lambrecht, N., Wittkop, C., Harding, C., Katsev, S., Torgeson, J., Poulton, S.W.,
711 2020. The biogeochemistry of ferruginous lakes and past ferruginous oceans. Earth Sci. Rev.
712 211, 103430. DOI: 10.1016/j.earscirev.2020.103430
713 Xie, X., Li, M., Littke, R., Huang, Z., Ma, X., Jiang, Q., Snowdon L. R., 2016. Petrographic and
714 geochemical characterization of microfacies in a lacustrine shale oil system in the Dongying Sag,

Jiyang Depression, Bohai Bay Basin, eastern China. Int. J Coal Geol., 165, 49–63. DOI: 10.1016/j.coal.2016.07.004

Xu, H., Hou, D., Löhr, S.C., Liu, Q., George, S.C., 2020. Early diagenetic pyrite cementation influences molecular composition of sedimentary organic matter in the Dongying Depression, China. Org. Geochem., 144, 104019. DOI: 10.1016/j.orggeochem.2020.104019

Zachos J. C., Dickens Gerald R., Zeebe Richard E., 2008. An early Cenozoic perspective on greenhouse warming and carbon-cycle dynamics. Science 451, 279–283. DOI: 10.1038/nature06588

Zeng, Z., Pike, M., Tice, M.M., Kelly, C., Marcantonio, F., Xu, G., Maulana, I., 2018, Iron fertilization of primary productivity by volcanic ash in the Late Cretaceous (Cenomanian) Western Interior Seaway. Geology 46, 859–862. DOI: 10.1130/G45304.1

Zhang, L., Wang, C., Wignall, P.B., Kluge, T., Gao, Y., 2018. Deccan volcanism caused coupled pCO_2 and terrestrial temperature rises, and pre-impact extinctions in northern China. Geology 46 (3), 271–274. DOI: 10.1130/G39992.1

Zhang, M., Liu, X., Li, A., Chang, X., Hu, L., Bi., N., Zhuang. G., Wang, H., 2024. Fate of terrigenous organic carbon within shelf sediments from the East China Sea controlled by sea-level and climatic changes since the last deglaciation. Palaeogeogr. Palaeoclimatol. Palaeoecol. 650, 112386. https://doi.org/10.1016/j.palaeo.2024.112386

Table and Figure captions

Table 1. Summary data of total organic carbon (TOC), organic carbon isotope composition ($\delta^{13}C_{org}$), total sulfur (TS), pyrite sulfur isotope ($\delta^{34}S_{py}$), Fe/Al ratio, and iron speciation of samples in the FY1 Well (data range, arithmetic average and number of samples, see Supplementary Table 1 for data points).

Figure 1. (A) Map of sites with existing MECO records on a paleogeographic reconstruction for the middle Eocene at 40 Ma (modified from Ploeg et al., 2023). (B) Simplified geological map of Bohai Bay Basin in western Pacific, showing the core location of FY-1 Well in the Jiyang Depression in eastern China (modified from Liang et al., 2016). (C) Stratigraphic column of the study interval in the middle Eocene. The Es_4^1 and Es_3^3 sediments are deposited during the rifting stage over 38–50 Ma ago

747 (modified from Shi et al., 2019).

748

749 Figure 2. Iron speciation, $\delta^{13}C_{org}$, TOC, and $\delta^{34}S_{py}$ values as a function of depth from
750 the middle Eocene (Es_4^1–Es_3^3) black shales in the Jiyang Depression (geological
751 timescale from Shi et al., 2019). (A) total organic carbon (TOC), (B) $\delta^{13}C_{org}$, (C) total
752 sulfur content (TS), (D) pyrite sulfur isotope ($\delta^{34}S_{py}$), (E) ratio of highly reactive Fe
753 to total Fe (Fe_{HR}/Fe_T), (F) ratio of pyrite iron to highly reactive iron (Fe_{py}/Fe_{HR}), (G)
754 content of pyrite iron, (H) content of carbonate iron. Note that Fe_{HR} =
755 $Fe_{py}+Fe_{ox}+Fe_{mag}+Fe_{carb}$, the thresholds for oxic versus anoxic (0.22–0.38) and
756 ferruginous versus euxinic conditions (0.6–0.8) are from Poulton et al. (2021); the
757 units of the study interval are based on lithological and geochemical differences, as
758 discussed in the text.

759

760 Figure 3. Plots of TOC vs TS, showing that the salinity of the most samples was similar
761 to the salinity of seawater, corresponding to ferruginous water conditions.

762

763 Figure 4. Plots of (A) Fe_{HR}/Fe_T vs Fe_{py}/Fe_{HR}; (B) Fe_{carb} vs Fe_{py}; (C) Fe_{py}/Fe_{HR} vs $\delta^{34}S_{py}$;
764 (D) TOC vs SRI.

765

766 Figure 5. Microscopic features of volcanic ash in the Middle Eocene shale of the Jiyang
767 Depression. (A) ostracod fragments in shales; (B) interbedded tuffs and shale; (C)
768 interbedded tuffs and shale with micro fractures; (D) pyroclastic interlayer in shales.

769

770 Figure 6. Sedimentary model of the paralic lake basin in the Jiyang Depression

developed in this study. (A) High primary productivity during middle Eocene long-time warmth. (B) Impacts of different geological events on organic carbon burial. During a short period of cooling caused by volcanism, despite potential external sulfur inputs, bacterial sulfate reduction sufficiently depleted the sulfate pool to have created ferruginous conditions.

Figure 1

Click here to access/download;Figure;Fig.1.tif

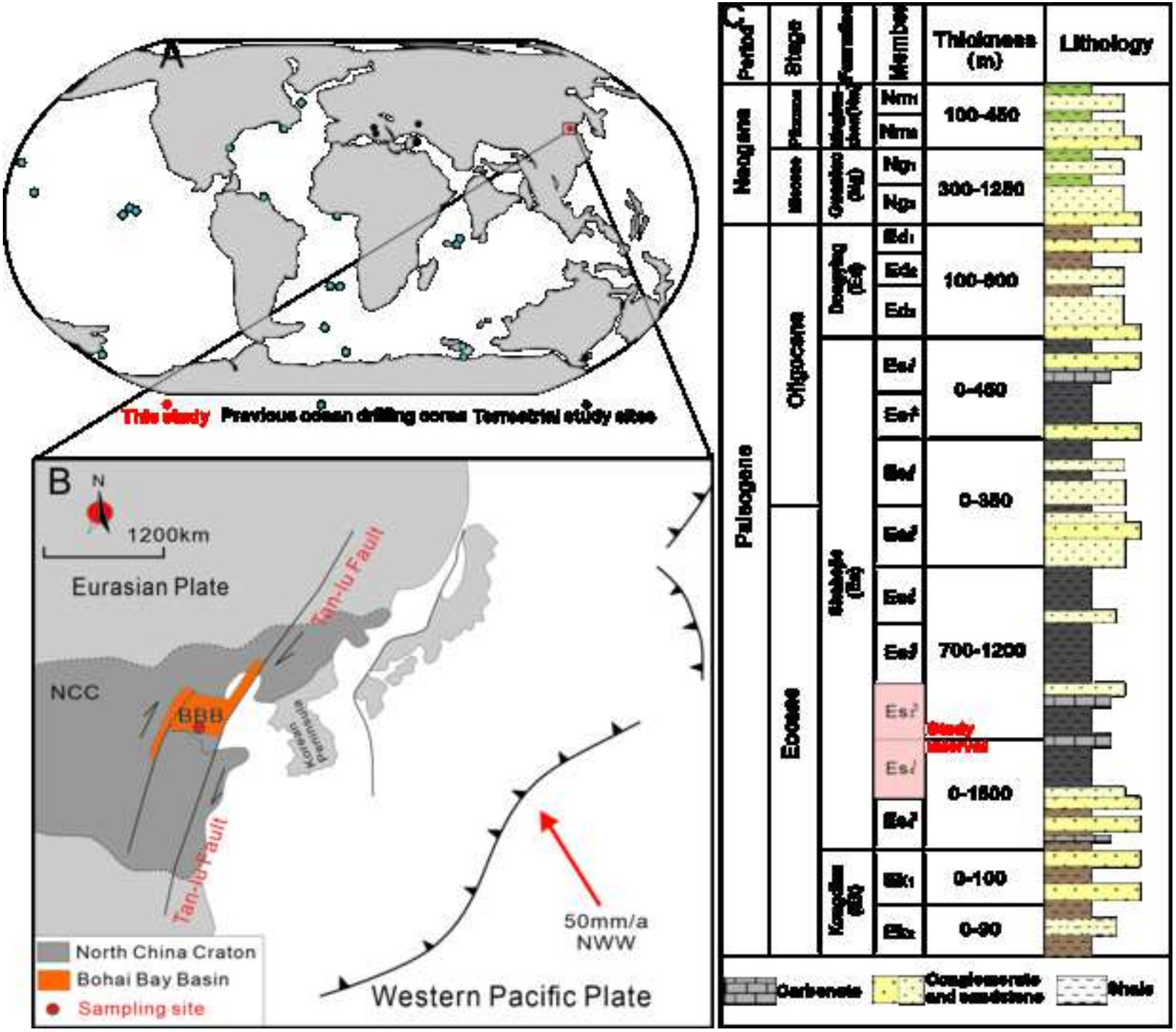

Figure 2

Click here to access/download;Figure;Fig.2.tif

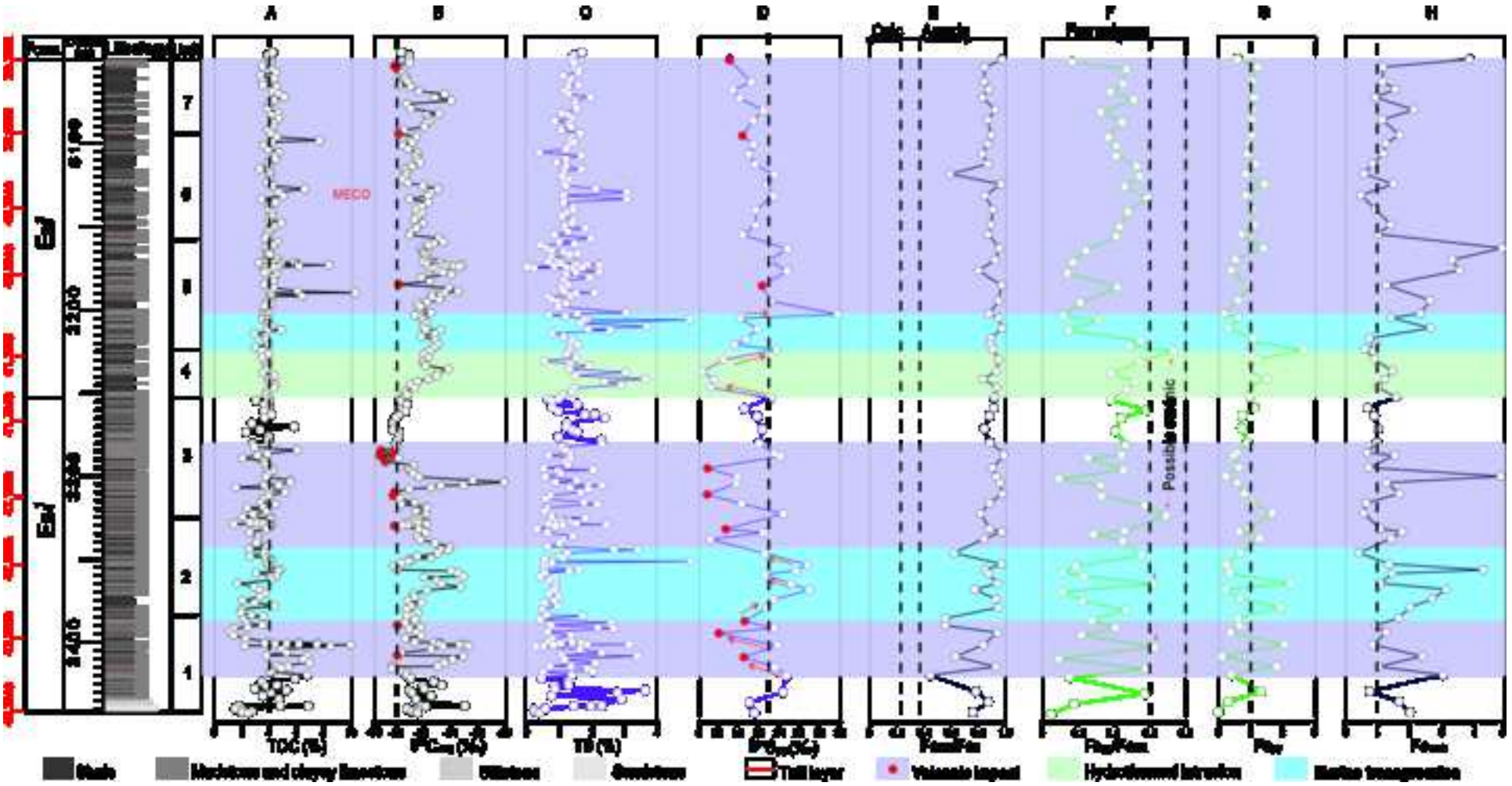

Figure 3

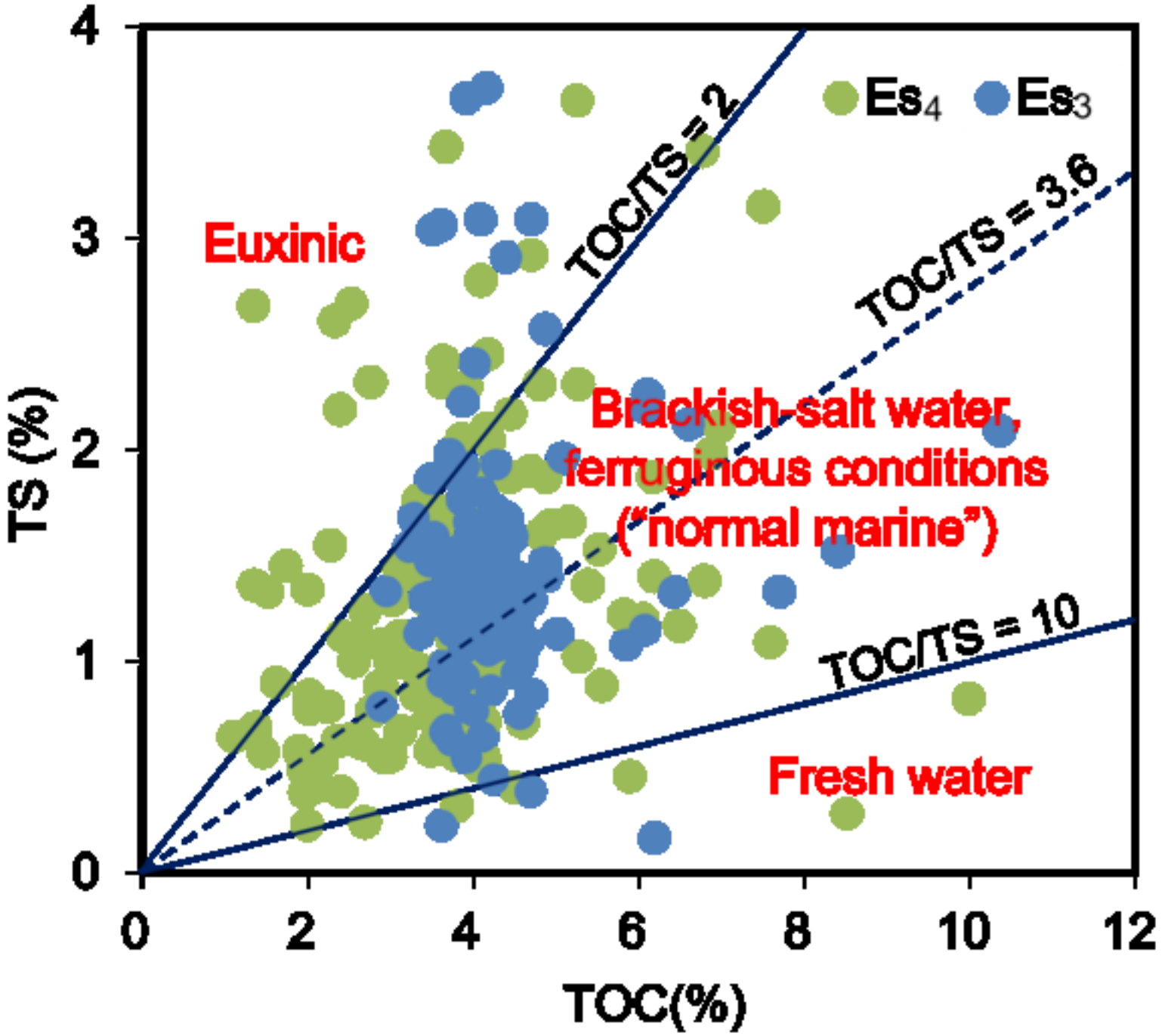

Figure 4

Click here to access/download;Figure;fig4.tif

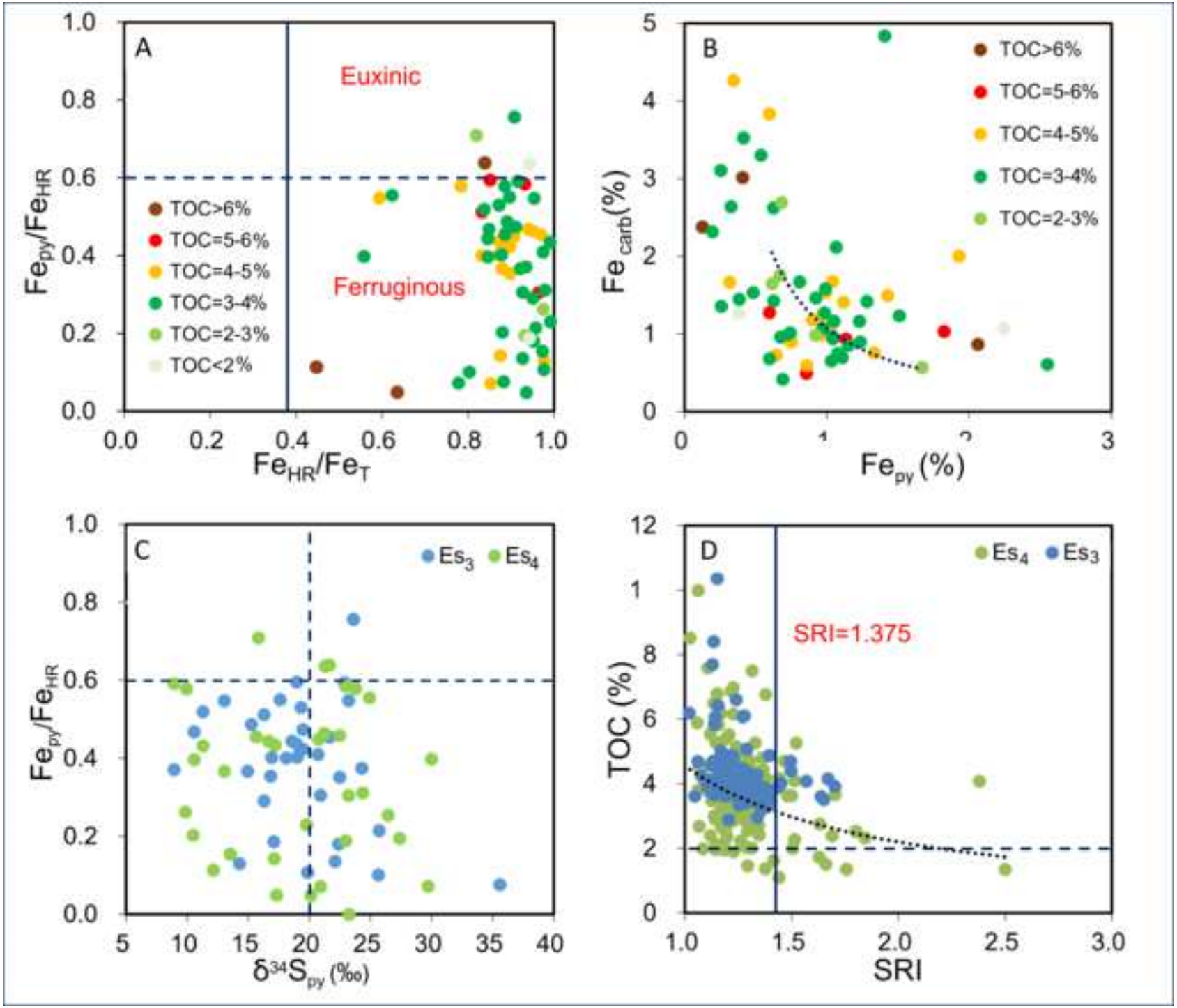

Figure 5

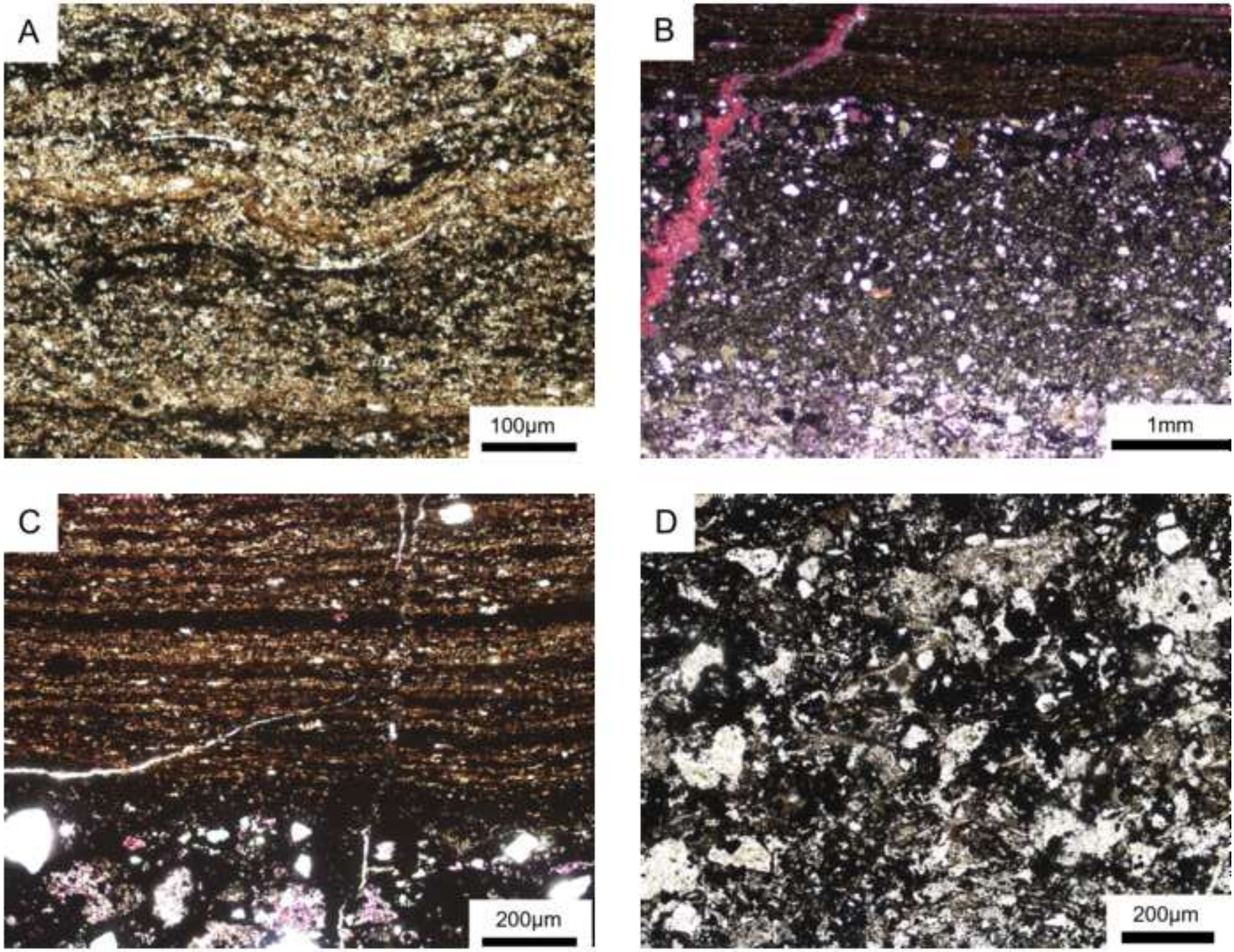

Figure 6

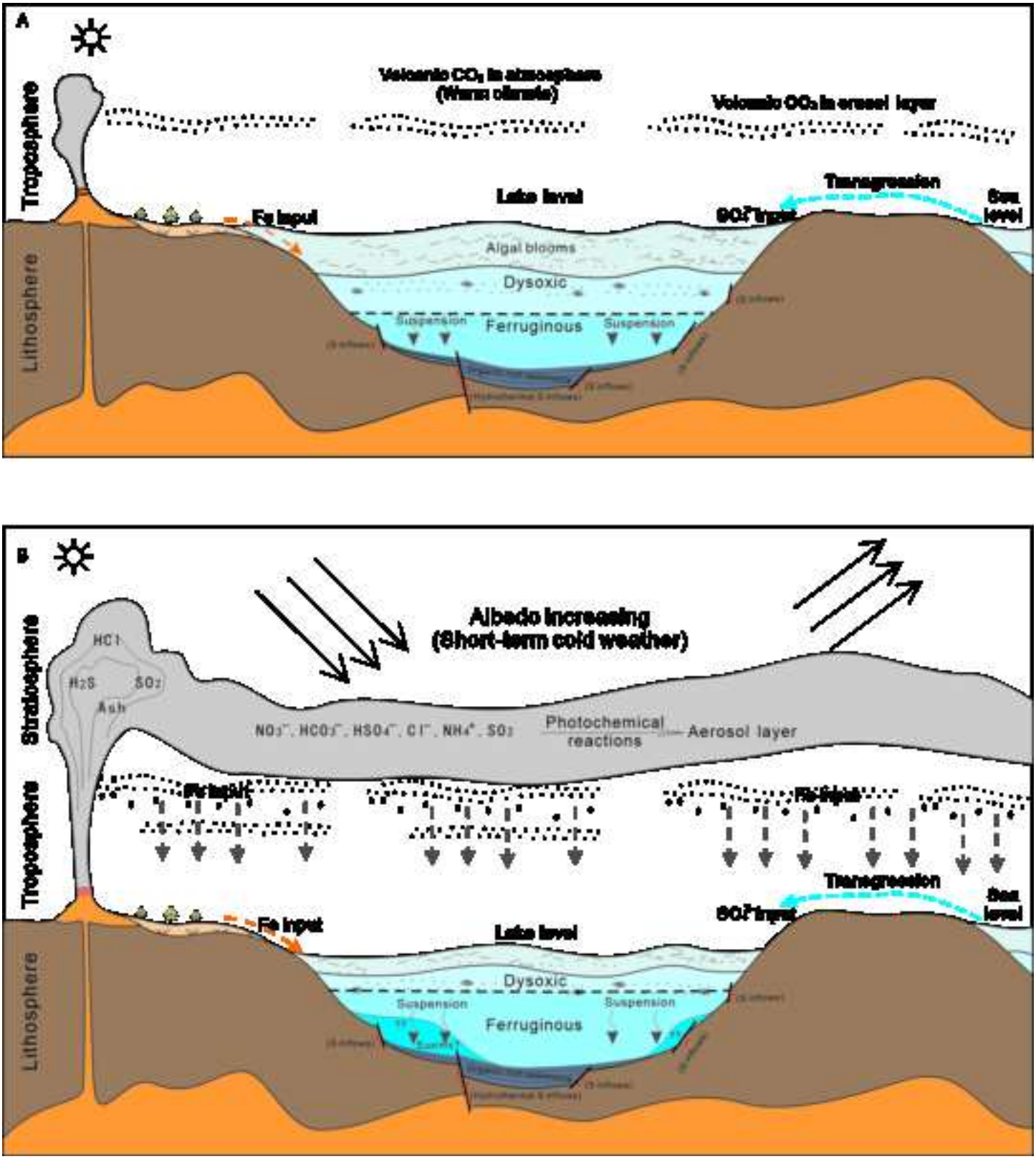

Declaration of interests

☒ The authors declare that they have no known competing financial interests or personal relationships that could have appeared to influence the work reported in this paper.

☐ The author is an Editorial Board Member/Editor-in-Chief/Associate Editor/Guest Editor for *[Journal name]* and was not involved in the editorial review or the decision to publish this article.

☐ The authors declare the following financial interests/personal relationships which may be considered as potential competing interests: